THE ASTROPHYSICAL JOURNAL, 468:350–368, 1996 September 1

THEORETICAL MODELS FOR ASTEROSEISMOLOGY OF DA WHITE DWARF STARS

P. A. BRADLEY[1]
XTA, MS B220, Los Alamos National Laboratory, Los Alamos, NM 87545
Received 1994 July 18; accepted 1996 March 14

ABSTRACT

Because white dwarfs are the most common end state of stellar evolution, determining their internal structure will yield many clues about the final stages of stellar evolution and the physics of matter under extreme conditions. We present the results of our parametric survey of evolutionary models of compositionally stratified white dwarfs with hydrogen surface layers (DA white dwarfs) and provide a comprehensive set of theoretical *g*-mode pulsation periods for comparison to observations of pulsating DA white dwarfs. This survey complements the previous survey of helium atmosphere (DB) white dwarf periods of Bradley, Winget, & Wood.

We show how to use the periods of low-overtone and/or trapped modes to constrain the internal structure of pulsating DA white dwarfs by utilizing their sensitivity to the total stellar mass and the location of the hydrogen/helium transition zone. We use G117-B15A as an example to demonstrate the potential of our models for asteroseismology; we suggest that G117-B15A has a mass of 0.55 $M_\odot$ and a hydrogen layer mass of $\approx 1.5 \times 10^{-4} M_*$.

Subject headings: stars: evolution — stars: interiors — stars: oscillations — white dwarfs

1. INTRODUCTION

The hydrogen atmosphere (DA) white dwarfs are the subject of considerable controversy—and promise. Because DA white dwarfs comprise about 80% of all spectroscopically known white dwarfs, they hold the key to understanding diverse astrophysical problems. Examples run from understanding how stars lose mass as asymptotic giant branch stars and become white dwarfs (e.g., Iben 1989; D'Antona & Mazzitelli 1991) to determining the age of the local Galactic disk (Winget et al. 1987; Wood 1992). For many years, the exact mass of the surface hydrogen layer has been a matter of dispute, and there was no readily available way to determine its mass. The hydrogen layer can be up to $\sim 10^{-4} M_*$ thick, according to stellar evolution calculations (Iben & MacDonald 1985, 1986; Koester & Schönberner 1986; D'Antona & Mazzitelli 1991). However, almost any hydrogen layer mass thinner than this can be accommodated by current theoretical models, depending on exactly where within the helium shell flash cycle the final mass loss episode occurs (Iben 1989). Observations say that the hydrogen layer of cool ($\sim$10,000 K) white dwarfs must be greater than $10^{-12} M_*$ thick, or convection will mix the hydrogen into the underlying helium layer. This wide range of possible hydrogen layer masses makes it difficult to determine what progenitor or progenitors give rise to DA white dwarfs. The hydrogen layer mass uncertainty also produces an uncertainty of about 0.04 $M_\odot$ in the mean mass of DA white dwarfs (Bergeron, Saffer, & Liebert 1992) and an additional uncertainty of about 1.5 Gyr to the age of the local Galactic disk (Wood 1995).

A promising solution to determining the hydrogen layer mass lies within the pulsating DA white dwarfs, called DAV or ZZ Ceti stars. The 24 known DAV stars are multiperiodic DA white dwarfs pulsating in nonradial *g*-modes, with effective temperatures between 13,000 and 11,000 K. This temperature interval coincides with the point where hydrogen has an opacity maximum, and pulsation driving in these stars is due to a combination of the κ, γ mechanism interacting with the convection zone (Brickhill 1983, 1991). Observations suggest that as DA white dwarfs evolve and cool, they pulsate upon their passage through the instability strip (Wesemael et al. 1991; Bergeron, Wesemael, & Fontaine 1992; Kepler & Nelan 1993; Bergeron et al. 1995). Indeed, Bergeron et al. (1995) show that once the mass dependence of the hot edge of the instability strip is taken into account, every DA white dwarf within the instability strip pulsates. Even more recently, Kepler (1995) shows one star that apparently defies this trend; however, it could have an intrinsic amplitude too low to detect or an unfavorable viewing angle. The dominance of pulsators in the instability strip suggests that the DAV stars are otherwise normal DA white dwarfs, and what we learn about them should apply to the majority of DA white dwarfs. The DAV stars display a variety of pulsation behavior. The hotter DAVs, such as R548 (Stover et al. 1980), have roughly sinusoidal light curves and oscillate in only a few modes. GD 154 (Robinson et al. 1978; Pfeiffer et al. 1995) is representative of the cooler, strongly nonlinear pulsators. GD 154 has a complex light curve, with a pulsation spectrum dominated by harmonics and combination terms, resulting from the strongly nonsinusoidal pulse shapes of the linearly independent modes.

Multisite data exist for nine of the 24 known DAV stars, but seismological progress has been slow, mainly because of the difficulty in identifying a sufficient number of stable and *distinct* linear pulsation modes for seismological analysis. Multisite data are important, because they allow us to unambiguously identify the different overtone modes in the light curve and at least some of the "fine structure" peaks resulting from slow rotation and/or magnetic fields. Fontaine et al. (1992) and Bergeron et al. (1993) made the first attempts at seismology of DAV white dwarfs, considering G226–29 and GD 165, but they had to make assumptions about the identity of the shortest period mode to constrain the derived hydrogen layer mass. Clemens (1994) studied the pulsation periods of the DAV stars *as a class* and demonstrated that the periods of the hotter DAV stars cluster into distinct bands, indicating a common mode structure, and hence, a common composition profile.

[1] pbradley@lanl.gov

Clemens compared the periods to the models of Brassard et al. (1992b) and Bradley (1993) and was able to find a satisfactory fit when he identified most of the period bands as being $l = 1$ modes. Surprisingly, the implied hydrogen layer mass was of order $10^{-4}M_*$. Subsequently, Robinson et al. (1995) determined the identity of the 215 s mode of G117-B15A as an $l = 1$ mode, consistent with Clemens' assignment of it as the $l = 1$, $k = 2$ mode. Brassard et al. (1993) analyzed data on G117-B15A and suggest that all three dominant periods are $l = 1$ modes. However, Brassard et al. (1993) and Fontaine & Brassard (1994) appear to differ by identifying the 215 s period as the $k = 1$ mode, which gave them a hydrogen layer mass of $\sim 1 \times 10^{-6}M_*$. Put together, these recent results suggest the long standing controversy over "thick" ($M_H \sim 10^{-4}M_*$) versus "thin" ($M_H \lesssim 10^{-10}M_*$) hydrogen layer masses question is at last being answered. This knowledge, combined with the (necessarily) sparse sampling of previous model grids and the availability of a white dwarf evolution code that includes all of the latest input physics, provides us with strong motivation to undertake a new in-depth examination of the nonradial g-mode properties of a new generation of evolutionary DA models.

In the rest of this paper, we present an extensive grid of DA white dwarf models and provide period grids useful for asteroseismology. We examine the effect of changing the various structural parameters on the theoretical pulsation periods of our models and use this information to constrain the structure of G117-B15A. Finally, we summarize our results and describe their potential consequences for our understanding of white dwarf evolution.

2. THE EQUILIBRIUM MODELS

We use equilibrium models computed with the white dwarf evolution code (WDEC) described by Lamb & Van Horn (1975), Wood (1992), and Bradley, Winget, & Wood (1993) with suitable resolution and smoothness for pulsation analysis. These white dwarf models are essentially identical to the helium atmosphere models of Bradley et al. (1993), with the addition of a hydrogen surface layer over the now underlying helium layer. Here we give a brief description of the relevant features of our models and refer the reader to Wood (1992) and Bradley et al. (1993) for additional details.

We begin our evolutionary sequences with pure carbon core models of stars used by Kawaler, Hansen, & Winget (1985). They evolved these models from the main sequence to the planetary nebula nucleus stage, where we pick them up as our starter models. These models start at $\log L/L_\odot \sim 3$ and $T_{\rm eff} \gtrsim 10^5$ K, and we follow their evolutionary cooling down to effective temperatures of about 10,000 K, below the cool edge of the observed instability strip. We then extract models that lie within the observed instability strip—between 13,500 and 10,500 K—and pulsationally analyze them. We use 0.60 $M_\odot$ models for most of our examples for ease of comparison with the published results of others, and because this mass is close to the observed mean mass for hot DA white dwarfs of 0.56 $M_\odot$ (Bergeron et al. 1992). However, we examine models ranging from 0.40 to 1.05 $M_\odot$ to cover most of the DA mass range between 0.45 and 1.20 $M_\odot$ of Bergeron et al. (1992).

Observations place only modest constraints on the structural details for DA models, potentially leaving us with a very large volume of parameter space to explore. We place the following restrictions on the composition profiles of our models to make our calculations feasible. There are no rigorous constraints on the composition profile of the C/O core, so we consider compositions ranging from pure carbon to pure-oxygen. For mixed C/O cores, we use simplified profiles such as those described by Wood (1992) and shown in Figure 1. We change the location of the C/O composition gradient and the C/O mass ratio separately to distinguish the observable consequences of each. Our models have hydrogen layer masses of $10^{-6}M_*$ or greater, because of recent interpretations of observed pulsation periods.[2] We cover several hydrogen layer masses for each stellar mass in anticipation that there may be a modest range of hydrogen layer masses for a given stellar mass, and also because we expect the maximum hydrogen layer mass to decrease with increasing stellar mass (D'Antona & Mazzitelli 1979). We always make the helium layer at least 100 times more massive than the hydrogen layer to avoid overlapping transition regions (see Arcouragi & Fontaine 1980). When $M_H < 10^{-4}M_*$, we set $M_{He} = 10^{-2}M_*$ to facilitate comparisons of pulsation properties due to changes in the hydrogen layer mass.

By the time our DA models reach the observed instability strip, they are $\gtrsim 4 \times 10^8$ yr old, which is greater than the time theoretically required for diffusion to reach equilibrium at the H/He interface. Therefore, we model the H/He transition zone with a double exponential chemical composition profile corresponding to diffusive equilibrium. In contrast, we make the He/C transition zone somewhat steeper than diffusive equilibrium predicts to avoid having helium present in the center of the model, which contradicts the expectation that nuclear burning should consume all of the helium nuclei during core helium burning. Also, the helium "tail" lies within strongly degenerate material where diffusion is suppressed. For these reasons, we use a "thin" He/C transition zone (Fig. 1, *long-dashed line*), unless otherwise specified.

We use the Böhm & Cassinelli (1971) version of convection with the mixing length–to–pressure scale height ratio set to 2 (≡ML3 convection). This gives the best match between the theoretical and observed hot edge of the instability strip according to Bradley & Winget (1994a) and Fontaine, Brassard, & Wesemael (1994). However, we emphasize that our choice of mixing-length theory has little effect on the theoretical pulsation periods, as shown by Brassard et al. (1992b).

To compute our theoretical pulsation periods, we use the same Runge-Kutta-Fehlberg (RFK) pulsation analysis tools as Bradley et al. (1993). We refer the reader to that paper for details, commenting only on the differences in the behavior of our DA model results. Our RKF program computes the eigenvalue period, along with a variational method period from the eigenfunctions. These periods computed by these two methods normally agree to better than 0.1%, but a few of the low-overtone modes in our models with $M_H \sim 10^{-4}M_*$ have differences of several percent between the eigenvalue and variational method periods. This difference is due mainly to errors in the eigenfunctions resulting from the "shooting" technique used to solve the pulsation equations. To confirm this, we look at otherwise identical models that have different resolutions, i.e., 300,

[2] We can create models with thinner hydrogen layers, should the need arise. See Bradley & Winget 1991 and Brassard et al. 1992a for examples.

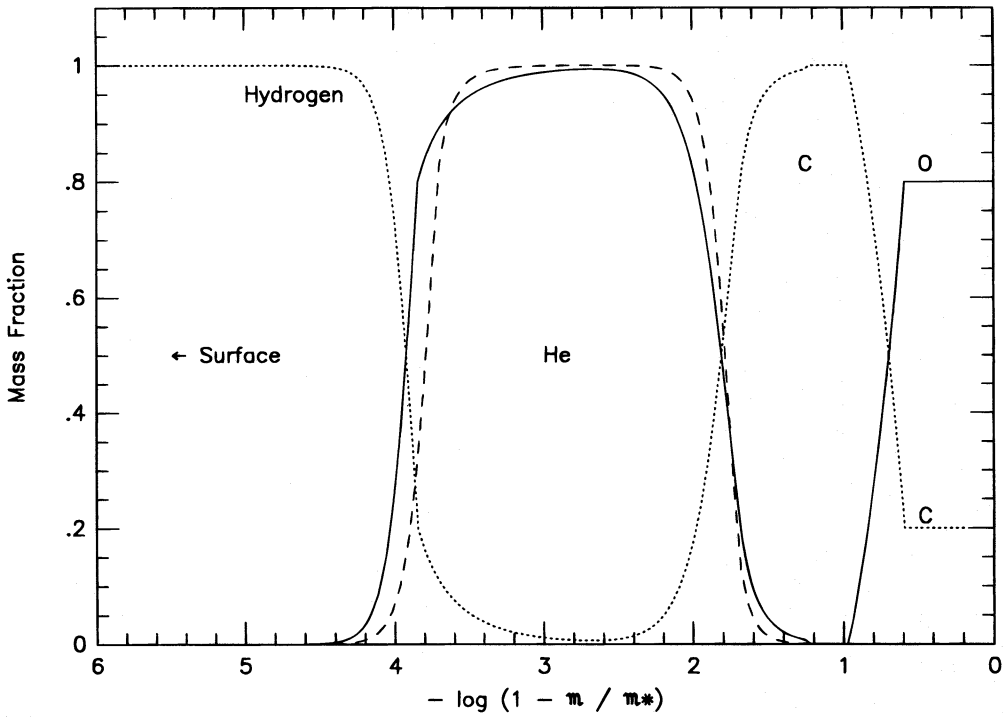

FIG. 1.—Schematic of the composition profile used in our models. The solid line shows the helium abundance profile in normal models, and the long-dashed line shows the helium profile for models with thin H/He and/or thin He/C composition transition zones. The core of this model is 80% oxygen out to $0.75M_*$, and it changes to pure carbon by $0.90M_*$.

400, or 500 total zones. Here the difference between the eigenvalue periods is at most 1% for trapped modes and generally is less than 0.2% otherwise. We infer this to be the true error in our eigenvalue periods.

The periods of our models are similar to those of Bradley & Winget (1991) and Brassard et al. (1992b); the differences in periods are due to differences in the structure of the equilibrium models. As a check on the periods of our models, we compare the periods of our carbon core 0.60 $M_\odot$ models with $M_H = 10^{-4}M_*$ and $M_{He} = 10^{-2}M_*$ to the results of Bradley & Winget (1991) and Brassard et al. (1992b). We find that the gross period structure is similar, but the Tassoul, Fontaine, & Winget (1990) model periods are systematically shorter, with a typical difference of 15%. The differences in the pulsation periods, mode trapping properties, and cooling rates are due to our use of a more realistic equation of state (EOS) that has lower heat capacities. As noted by Bradley, Winget, & Wood (1992), this makes our models cool faster, and the age difference is consistent with the difference between the average period spacing between consecutive overtone modes. We confirm that the age difference is the dominant effect by examining models that do not have chemical composition gradient effects in the Brunt-Väisälä frequency. The period agreement of most modes in the two models is better, but the Tassoul et al. (1990) models still have systematically lower periods. Fontaine & Brassard (1994) investigate the changes in theoretical periods produced by various changes in the input physics. Our most serious omission (not using OPAL opacities) produces only about a 1% change in the pulsation periods at 1000 s. Based on our comparison, we believe our models are the best currently available evolutionary grid for a systematic exploration of the pulsation properties of DAV white dwarfs.

3. OVERVIEW OF PERIOD TRENDS IN DA MODELS

This section is for people wishing a quick overview of the relative importance that changes in the structure of our DA models have on the theoretical periods without going into all of the details required for accurate seismology of individual objects. Here we provide a brief description of the general pulsation properties of white dwarf g-modes and schematically illustrate the effect our structural changes have on the theoretical period trends. Much of this material is covered in detail by Bradley & Winget (1991) and Brassard et al. (1992a, 1992b), and we recommend these papers to those wishing additional details about DA white dwarf g-mode properties.

We describe the angular dependence of the g-mode eigenfunctions in terms of spherical harmonics with indices l and m. We cannot resolve the disk of any white dwarf, so geometric cancellation effects become increasingly severe as the l value increases (Dziembowski 1977). In practice, we are not likely to see modes with $l \geq 3$, and we only compute results for $l = 1, 2$, and 3 g-modes. We do not present results for our $l = 3$ modes here; they have the same general behavior as the $l = 1$ and 2 modes, albeit at 1/2.46 the period of the corresponding $l = 1$ mode.

3.1. *Basic g-Mode Properties*

Before we probe the details of white dwarf pulsation properties, we wish to recall a few properties of white dwarf g-modes. Because buoyancy is the restoring force, the Brunt-Väisälä frequency is the most important quantity affecting the pulsation spectrum of a white dwarf model. Three features dominate the Brunt-Väisälä frequency of a typical DA model (see Fig. 2). First, the Brunt-Väisälä frequency is quite small in the strongly degenerate core of a

model, which causes the pulsation periods to be long compared to the dynamical timescale. It also concentrates most of the oscillation energy of a g-mode into the outer layers of a model. There are also three peaks in the Brunt-Väisälä frequency near $10^{-1}M_*$, $10^{-2}M_*$, and $10^{-4}M_*$ associated with the C/O, He/C, and H/He composition transition zones. These play a crucial role in modifying the period structure by acting as "filters" that can affect the character of selected modes by "trapping" their oscillation energy close to the surface or "confining" it in the core. (Note: We borrow the notation of Brassard et al. 1992b, and highly recommend this paper and Brassard et al. 1992a for further discussions on mode trapping and confinement.)

Mode trapping, described by Brassard et al. (1992a) and Bradley et al. (1993) plays a decisive role in determining the period structure of ZZ Ceti white dwarfs. As Bradley & Winget (1991) and Brassard et al. (1992a, 1992b) show, an eigenfunction with a wavelength similar to the physical depth of a chemical composition gradient can get "pulled" into a mechanical resonance where the wavelength and physical depth of the composition gradient match. This resonant interaction is called mode trapping, and the affected modes are called trapped modes. Neighboring modes are also "pulled" toward this resonance, and the result is adjacent overtone modes with periods much closer together than average. The mode trapping in which we are most interested confines the eigenfunction oscillations between the composition gradient and the surface of the white dwarf. The eigenfunction amplitude is small in the core; this causes trapped modes to have a local minimum in kinetic energy compared to neighboring modes. Because trapped modes require less energy to oscillate with a given amplitude, one might expect that trapped modes with periods close to the thermal timescale at the base of the driving region (see Bradley & Winget 1994a) will have the largest amplitudes and be preferentially seen. We caution that while this is a popular explanation, it is *unproven*. Of less concern to us are modes trapped within the core, called confined modes by Brassard et al. (1992a, 1992b). These modes have higher than average kinetic energies, and we expect them to have smaller amplitudes, if they are visible at all.

3.2. *Brief Summary of Period Trends Versus Structural Changes*

We will now illustrate the period changes caused by varying the structure of our models by using Figure 3 and the following outline. Changes in the hydrogen layer mass and the total stellar mass produce the largest changes on the pulsation mode spectrum. Other changes, such as varying the helium layer mass, the thickness of the composition transition zones, the C/O mass fraction in the core, and the location of the C/O inner transition point, produce smaller effects. In Figure 3 we use $l = 2$ modes to illustrate these trends; they are the same for other l values, and we have enough $l = 2$ modes in the period range of 100–800 s to adequately show trends at low and high overtones. Below, we describe the most important effects of each structural change. We describe subtle effects and detailed physical explanations in the next section.

1. *Increase the hydrogen layer mass.*—This shortens all of the pulsation periods and causes a slight drop in the mean period spacing between modes, shown in Figure 3*a*. The model with $M_H = 10^{-6}M_*$ has 3–4 modes between minima, with 10–15 s difference between period spacing minima and maxima. This cyclical behavior in the period spacing is the result of mode trapping by the hydrogen

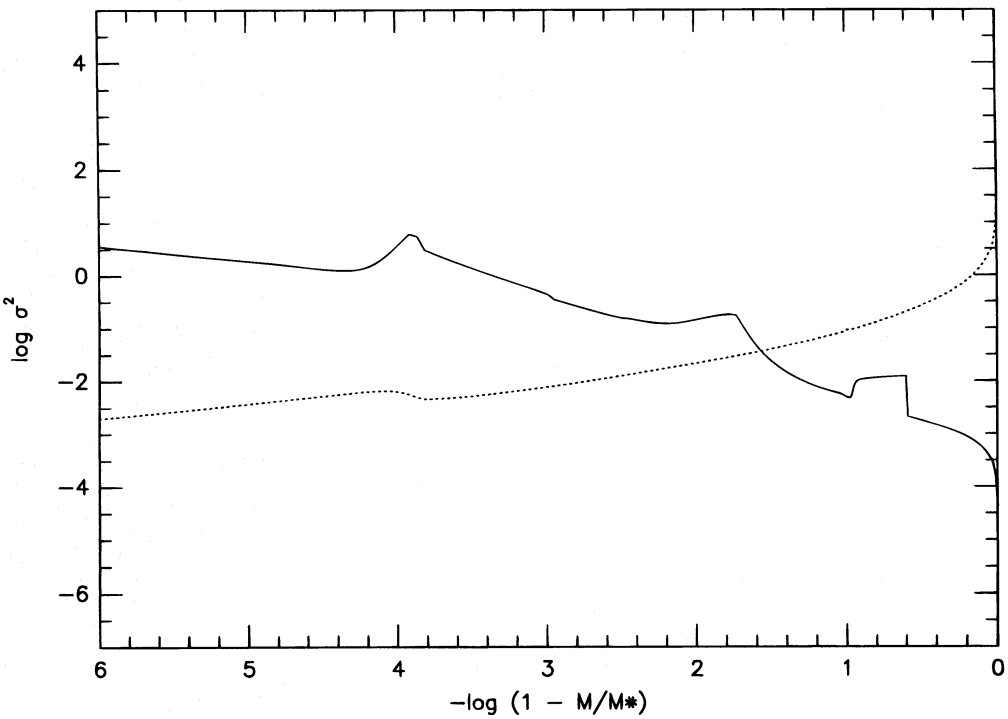

FIG. 2.—Propagation diagram for the model shown in Fig. 1. The peaks in the Brunt-Väisälä frequency (*solid line*) from the center (*at right*) are caused by the C/O, He/C, and H/He chemical composition gradients, respectively.

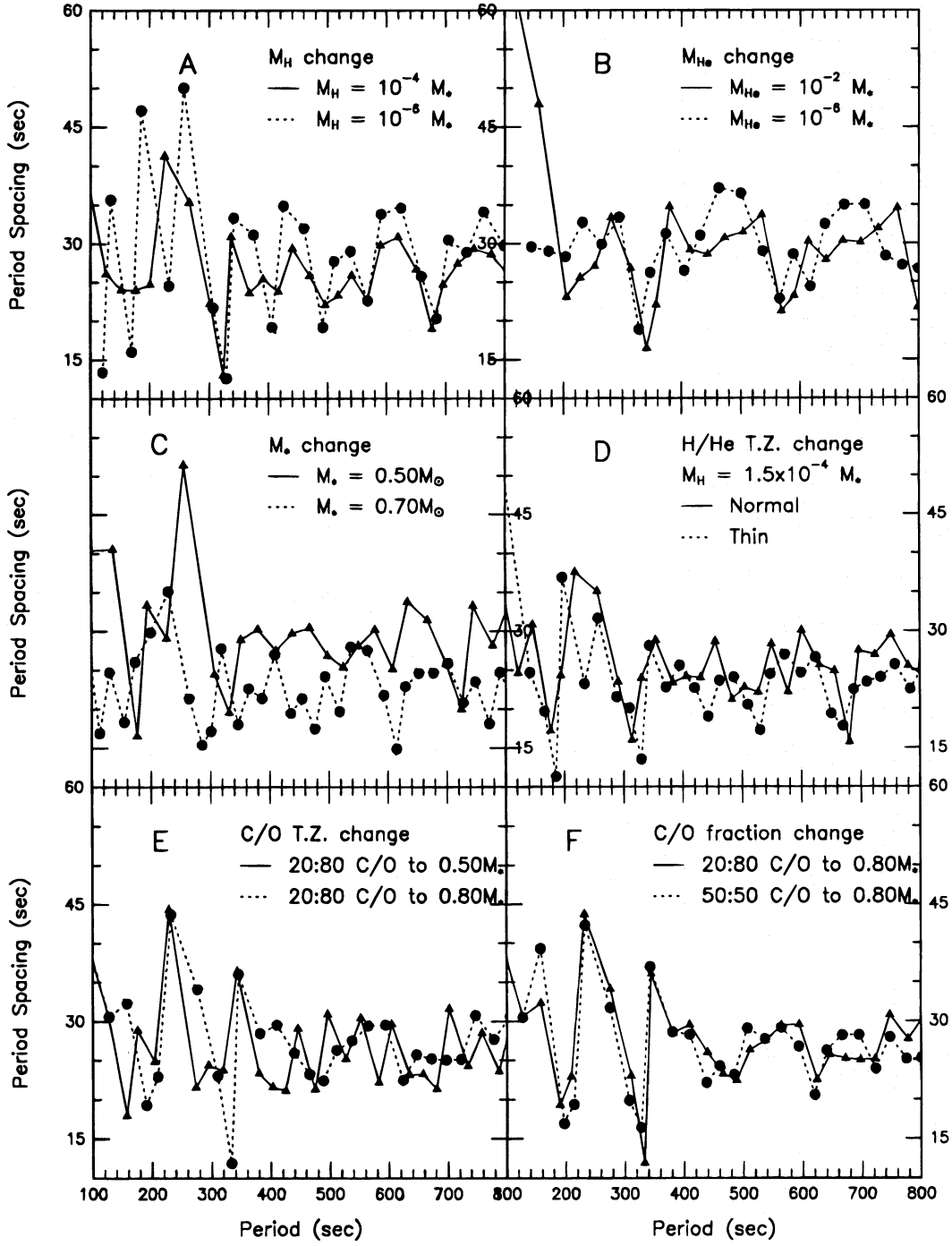

FIG. 3.—Six-panel summary describing the effect that changing various structural features has on the period spectrum, measured here by the period spacing between consecutive overtone modes. (*a–f*) show the effect of increasing M_H, increasing M_{He}, increasing M_*, making the H/He transition zone thinner, making the C/O transition region thinner, and increasing the oxygen fraction in the C/O core, respectively. (Consult the text for details.)

layer. When $M_H = 10^{-6}M_*$, the hydrogen layer depth is nearly optimal for mode trapping, and any mode trapping resulting from the helium layer or the C/O core is small. When $M_H = 10^{-4}M_*$, mode trapping by the hydrogen layer is less effective, and mode trapping by the other layers produces an irregular looking period spacing pattern. Deeper minima can (and do) occur when a mode has a mode trapping resonance with more than one layer; examples are the minima near 320 and 680 s.

2. *Increase the helium layer mass.*—When $M_{He} = 10^{-2}M_*$, mode trapping by the helium layer makes the $k = 1$ period shorter without seriously affecting the $k = 2$ and 3 modes, resulting in the off-scale period spacing of 78.2 s (see Fig. 3*b*). When $M_{He} = 10^{-6}M_*$, the helium produces additional mode trapping, which we see as additional, shallower period spacing minima compared with the $M_{He} = 10^{-2}M_*$ plot. Helium is a more transparent material than hydrogen, so when we increase the helium layer mass, we increase the cooling rate of our models. As a result, the higher overtone ($k \gtrsim 11$) modes show increasingly longer periods at the same effective temperature when we increase the helium layer mass.

3. *Increase the total stellar mass.*—Increasing the total stellar mass acts to decrease the Brunt-Väisälä frequency in

TABLE 1

PERIODS FOR LOW-OVERTONE MODES OF MODELS NEAR 12,500 K
$M_H = 1.5 \times 10^{-4} M_*$ AND $M_{He} = 1.5 \times 10^{-2} M_*$

l, k	0.40 $M_\odot$ log g = 7.58 12,620 K	0.50 $M_\odot$ log g = 7.80 12,500 K	0.55 $M_\odot$ log g = 7.90 12,440 K	0.60 $M_\odot$ log g = 7.99 12,440 K	0.65 $M_\odot$ log g = 8.07 12,620 K	0.70 $M_\odot$ log g = 8.15 12,700 K	0.75 $M_\odot$ log g = 8.23 12,500 K	0.80 $M_\odot$ log g = 8.31 12,440 K
1, 1	186.6	158.4	146.9	136.7	122.8	118.7	111.7	105.1
1, 2	235.2	221.0	212.9	203.7	193.7	182.5	173.8	164.1
1, 3	315.4	290.6	270.7	251.5	227.0	216.0	201.4	187.2
1, 4	354.6	310.9	297.4	282.9	267.2	250.4	236.5	221.5
1, 5	420.7	376.1	354.9	333.0	306.3	289.2	270.9	253.0
1, 6	487.7	424.2	397.6	374.5	365.0	333.6	315.7	298.3
1, 7	507.9	489.1	471.5	441.0	404.5	381.6	356.9	334.2
1, 8	591.3	515.5	485.6	466.2	443.1	421.3	406.3	386.1
1, 9	644.5	568.2	537.8	506.3	466.8	443.5	416.9	394.0
1, 10.....	701.5	630.2	587.4	549.6	519.2	483.2	458.0	432.3
1, 11.....	755.0	683.0	649.4	609.1	563.3	528.6	496.6	465.9
1, 12.....	800.5	725.8	686.7	650.4	610.1	576.6	543.2	510.6
1, 13.....	855.6	766.3	729.2	689.1	643.2	605.9	573.6	543.0
1, 14.....	903.7	815.5	768.2	724.3	679.2	640.6	606.0	570.9
1, 15.....	972.9	853.9	813.7	769.0	716.9	674.0	636.4	598.7
2, 1	108.2	91.7	85.0	79.1	71.0	68.7	64.6	60.8
2, 2	139.5	131.2	126.5	121.2	115.5	108.9	103.8	98.2
2, 3	195.9	169.8	157.3	145.9	131.6	125.3	116.8	108.7
2, 4	208.9	193.2	185.5	176.4	167.0	156.1	147.1	137.7
2, 5	246.9	219.9	207.0	193.8	177.5	167.9	157.1	146.6
2, 6	289.0	246.0	230.6	217.2	211.5	193.3	182.2	172.6
2, 7	328.0	295.5	274.9	255.4	234.5	220.7	206.3	193.2

the C/O core and increase it in the outermost layers, causing the periods and period spacings to decrease (see Fig. 3*c*). The number of overtones between trapped modes (period spacing minima) changes more slowly, so the 0.50 $M_\odot$ trapped modes at $k = 8$ (332 s) and $k = 22$ (725 s) are the 0.70 $M_\odot$ trapped modes at $k = 9$ (286 s) and $k = 24$ (615 s). The average period spacing between modes drops from 29.5 s for 0.50 $M_\odot$ to 23.2 s for 0.70 $M_\odot$.

4. *Make the* H/He (*or* He/C) *transition zone thinner.*—A thinner transition zone increases the density gradient in the transition zone and accentuates mode trapping. Figure 3*d* shows the expected result; the period spacing minima are deeper in the model with a thin H/He composition transition zone. There are also extra period spacing minima in the thin transition zone model because the increased mode trapping efficiency of the hydrogen layer starts to "drown out" mode trapping due to the He/C and C/O transition zones. Although we do not show a plot, making the He/C transition zone thinner has a similar effect, but it affects different overtone modes.

5. *Move the C/O inner transition zone outward.*—We keep the location where the C/O core turns to pure carbon at $0.90 M_*$, so moving the inner C/O transition point outward in the model makes the C/O transition region thinner, which enhances mode trapping. The enhanced mode trapping of the C/O interface affects the interplay of mode trapping resonances caused by the C/O, He/C, and H/He interfaces. In this case, Figure 3*e* shows that the model with the inner transition point at $0.80 M_*$ has fewer, deeper minima because the resonances of the three interfaces are more "in phase," while our other example has a more jagged structure. At low overtones, the trapped mode at $k = 3$ changes to $k = 4$ as we make the C/O transition region thinner, and the period spacings between $k = 6$ and 8 are affected.

6. *Increase the oxygen mass fraction of the core.*—Increasing the oxygen mass fraction of the core has little effect on the mode trapping properties of the model, and the period spacing plots in Figure 3*f* exemplify this point. The two models in our illustration have sufficiently similar C/O mass ratios that the slightly longer periods we expect in the (older) more oxygen-rich model are not noticeable.

4. DETAILS OF PERIOD TRENDS IN DA MODELS

In this section we describe the trends in our theoretical pulsation periods as we change various model parameters most useful for asteroseismology. This section is an expansion of the previous subsection, and we describe how much the pulsation periods of affected modes vary as we change the structural properties of our DA models one by one. We provide a detailed grid of DA model periods as a function of stellar mass and hydrogen layer mass for two different effective temperatures. These tables provide period information for the most important structural changes; we also describe in detail the effect other structural changes have on our theoretical periods and the modes that are most affected. We anticipate that this section will be most useful for people wishing to perform seismology of individual ZZ Ceti stars. We compute model sequences with masses between 0.40 and 1.05 $M_\odot$ to cover the entire mass range likely to be relevant for observed pulsating DA white dwarfs. Our pulsation period grids for DA white dwarf models cover hydrogen layer masses ranging from $M_H = 1.5 \times 10^{-4} M_*$ to $5 \times 10^{-6} M_*$ for several stellar masses. We present these results[3] for models with effective temperatures near 12,500 and 11,700 K in Tables 1–12. In this section we wish to determine the relative importance of each structural change, the absolute size of the changes, and how they affect our seismological interpretation of observed DAV stars. Here we emphasize pulsation periods, rather than period spacings, because we see so few pulsation modes in any one ZZ Ceti star up to now. When many modes are discovered in a

[3] Tables with kinetic energies, first order rotation splitting coefficients ($C_{l,k}$), and tables for other chemical composition profiles are available from the author via e-mail.

TABLE 2

PERIODS FOR LOW-OVERTONE MODES OF MODELS NEAR 11,700 K
$M_H = 1.5 \times 10^{-4}\ M_*$ AND $M_{He} = 1.5 \times 10^{-2} M_*$

l, k	0.40 $M_\odot$ log g = 7.59 11,670 K	0.50 $M_\odot$ log g = 7.81 11,860 K	0.55 $M_\odot$ log g = 7.90 11,530 K	0.60 $M_\odot$ log g = 7.99 11,720 K	0.65 $M_\odot$ log g = 8.07 11,780 K	0.70 $M_\odot$ log g = 8.15 11,880 K	0.75 $M_\odot$ log g = 8.23 11,750 K	0.80 $M_\odot$ log g = 8.31 11,750 K
1, 1	190.7	160.6	150.5	139.4	125.8	121.6	114.5	107.0
1, 2	246.5	227.4	221.0	209.4	199.9	188.1	177.8	167.6
1, 3	333.1	295.6	276.7	255.7	231.2	219.8	204.8	189.9
1, 4	362.9	319.4	308.8	290.8	275.5	257.6	242.1	225.9
1, 5	435.5	384.0	364.6	339.5	312.2	295.0	276.1	257.4
1, 6	507.2	431.7	409.2	383.6	375.9	343.8	324.4	305.1
1, 7	535.1	507.8	485.2	449.2	416.1	390.1	364.7	340.7
1, 8	610.5	525.4	510.9	486.4	464.5	441.2	420.8	394.3
1, 9	663.4	581.4	554.9	518.3	478.7	454.7	430.5	409.5
1, 10.....	738.2	640.4	602.6	561.9	532.9	497.4	470.0	441.3
1, 11.....	779.9	701.2	668.9	621.5	578.6	540.3	507.6	475.4
1, 12.....	837.2	742.4	711.1	668.4	626.7	592.0	555.9	520.2
1, 13.....	887.8	786.5	756.0	707.1	665.0	624.3	589.4	556.0
1, 14.....	936.1	833.3	793.7	744.6	699.2	659.5	622.1	583.6
1, 15.....	1002.8	877.2	845.8	789.4	740.6	694.2	653.5	613.0
2, 1	110.5	92.9	87.0	80.6	72.8	70.3	66.2	61.9
2, 2	146.1	135.0	131.3	124.5	119.2	112.3	106.2	100.3
2, 3	202.9	172.2	160.6	148.3	134.1	127.5	118.8	110.3
2, 4	217.2	198.8	192.4	181.8	171.8	160.3	150.4	140.2
2, 5	255.2	224.3	212.4	197.5	181.0	171.2	160.0	149.1
2, 6	295.1	250.3	237.3	222.5	217.6	199.1	187.8	176.5
2, 7	345.8	300.2	281.1	259.9	241.1	225.6	210.9	196.9

ZZ Ceti star, one can compute period spacings from the tabulated periods for comparison to observations. We compare the pulsation spectra of models with nearly identical temperatures, to avoid adding the effect of evolutionary cooling to the pulsation spectra. We describe the effects of different structural changes under separate subheadings to make them easier to locate. We use the three observed periods (at 215.2, 270.4, and 304.0 s) of G117-B15A to illustrate the observable consequences of each structural change, and in our final subsection we combine our results to constrain the structure of G117-B15A for several assumed mode identifications.

4.1. *Effects of the Hydrogen Layer Mass*

The mass of the hydrogen layer has the greatest effect on the pulsation spectrum of our DA models, making it the easiest parameter to determine seismologically. Decreasing the hydrogen layer mass produces two main effects. First, it increases the period of the first overtone mode and slightly increases the average period spacing between consecutive overtone modes. The first few overtone modes show a steady period increase with decreasing hydrogen layer mass until $\sim 10^{-8} M_*$ (see Fig. 4). Figure 4 also shows that the period spacing between low-overtone modes is insensitive

TABLE 3

PERIODS FOR LOW-OVERTONE MODES OF MODELS NEAR 12,500 K
$M_H = 1.0 \times 10^{-4} M_*$ AND $M_{He} = 1.0 \times 10^{-2} M_*$

l, k	0.50 $M_\odot$ log g = 7.81 12,530 K	0.55 $M_\odot$ log g = 7.90 12,820 K	0.60 $M_\odot$ log g = 7.99 12,620 K	0.65 $M_\odot$ log g = 8.07 12,740 K	0.70 $M_\odot$ log g = 8.15 12,560 K	0.75 $M_\odot$ log g = 8.23 12,760 K	0.80 $M_\odot$ log g = 8.30 12,740 K	0.85 $M_\odot$ log g = 8.39 12,680 K
1, 1	164.7	151.7	141.5	131.6	123.7	115.1	107.8	101.2
1, 2	227.1	216.7	209.7	199.4	191.1	179.7	169.9	159.5
1, 3	294.0	275.7	258.9	240.5	224.7	207.9	192.9	179.0
1, 4	311.9	290.9	277.7	261.7	248.4	231.6	216.9	202.4
1, 5	385.6	361.6	341.2	319.1	300.0	278.4	259.6	242.2
1, 6	437.8	406.6	383.6	360.8	344.8	322.5	304.8	288.9
1, 7	483.9	464.2	451.8	422.6	396.8	367.6	343.2	322.7
1, 8	530.7	491.1	462.5	439.5	424.7	400.9	383.0	365.2
1, 9	581.2	545.5	518.6	486.7	459.7	427.1	398.9	374.3
1, 10.....	644.6	599.3	563.4	527.4	500.0	468.0	441.1	417.0
1, 11.....	681.9	646.2	619.6	581.4	547.4	509.2	476.8	446.7
1, 12.....	738.4	688.5	652.2	614.9	587.6	549.8	518.1	486.4
1, 13.....	776.0	731.1	697.4	655.0	618.8	577.1	542.3	510.0
1, 14.....	821.2	771.9	734.2	690.8	657.4	613.8	576.9	541.4
1, 15.....	866.4	809.1	773.2	729.6	692.6	646.3	607.8	573.3
2, 1	95.3	87.7	81.8	76.1	71.5	66.6	62.3	58.5
2, 2	134.3	128.3	124.3	118.3	113.6	107.0	101.4	95.5
2, 3	175.6	161.8	150.8	139.9	130.5	120.8	112.2	104.2
2, 4	190.7	180.9	173.6	163.8	155.2	144.5	135.0	125.6
2, 5	224.5	210.1	198.0	184.9	173.6	161.1	150.1	140.0
2, 6	253.7	235.6	222.0	209.0	199.6	186.7	176.3	167.0
2, 7	304.5	282.2	263.5	244.8	229.5	212.5	198.4	186.5

TABLE 4

PERIODS FOR LOW-OVERTONE MODES OF MODELS NEAR 11,700 K
$M_H = 1.0 \times 10^{-4} M_*$ AND $M_{He} = 1.0 \times 10^{-2} M_*$

l, k	0.50 $M_\odot$ log g = 7.81 11,910 K	0.55 $M_\odot$ log g = 7.90 11,910 K	0.60 $M_\odot$ log g = 7.99 11,780 K	0.65 $M_\odot$ log g = 8.08 11,690 K	0.70 $M_\odot$ log g = 8.16 11,970 K	0.75 $M_\odot$ log g = 8.24 11,830 K	0.80 $M_\odot$ log g = 8.31 11,690 K	0.85 $M_\odot$ log g = 8.39 11,670 K
1, 1	167.1	154.9	144.6	135.3	126.0	118.2	111.4	104.2
1, 2	233.9	225.6	216.7	207.5	195.6	185.0	175.2	164.5
1, 3	301.2	283.0	264.4	246.4	227.9	212.1	197.4	182.9
1, 4	318.1	301.1	286.5	271.5	253.6	238.3	223.4	208.1
1, 5	393.6	372.0	349.5	327.9	304.6	284.7	266.4	248.5
1, 6	445.3	418.0	394.0	373.9	352.8	333.3	316.1	298.9
1, 7	504.1	490.1	464.4	433.9	403.4	376.6	353.7	333.0
1, 8	539.6	504.0	484.0	467.0	440.0	423.2	406.1	382.7
1, 9	594.6	563.5	533.1	502.0	468.2	437.9	412.6	392.5
1, 10.....	657.4	614.5	577.7	545.3	510.9	482.6	456.9	430.7
1, 11.....	701.2	672.2	638.0	599.6	557.2	522.6	491.8	461.2
1, 12.....	754.3	709.2	673.5	640.6	601.9	568.0	536.1	501.3
1, 13.....	796.5	758.3	718.8	677.6	631.5	595.0	562.9	529.6
1, 14.....	843.4	799.2	757.6	718.2	672.4	633.2	596.3	557.6
1, 15.....	884.2	839.8	802.4	759.8	709.0	667.6	630.1	593.3
2, 1	96.7	89.6	83.6	78.2	72.8	68.3	64.4	60.2
2, 2	138.4	133.6	128.4	123.2	116.4	110.2	104.6	98.5
2, 3	178.2	165.2	153.8	143.2	132.4	123.3	114.8	106.5
2, 4	196.1	187.8	179.1	169.6	158.2	148.4	138.7	128.7
2, 5	229.0	215.9	202.6	189.9	176.2	164.6	154.0	143.6
2, 6	258.0	242.1	228.2	216.5	204.2	192.8	182.8	172.7
2, 7	309.9	288.5	268.9	250.9	233.2	217.7	204.4	192.5

to the mass of the hydrogen layer, except when trapped mode identities change. When the hydrogen layer mass is less than $10^{-8} M_*$, the low-overtone mode periods are insensitive to changes in the hydrogen layer mass, because most of their pulsation energy lies below the hydrogen layer boundary.

Increasing the hydrogen layer mass also decreases the period interval between trapped modes (the trapping cycle), because mode-trapping resonances occur more frequently. For example, in carbon core models, about every fourth mode is trapped when the hydrogen layer mass is $10^{-6} M_*$, whereas about every other mode is trapped when the hydrogen layer mass is $\sim 10^{-4} M_*$. Also, when $M_H \sim 10^{-4} M_*$, the base of the hydrogen layer is so deep that only the first few overtone modes have sufficient mode energy down at the composition transition regions to show signs of strong mode trapping. When $M_H = 10^{-4} M_*$, models with He/C and C/O composition gradients show complicated period spacing plots (see Fig. 3*a*) resulting from a complicated interplay of mode-trapping resonances with the three chemical composition gradients. Only when $M_H \lesssim 10^{-6} M_*$ does mode trapping by the H/He composition gra-

TABLE 5

PERIODS FOR LOW-OVERTONE MODES OF MODELS NEAR 12,500 K
$M_H = 5.0 \times 10^{-5} M_*$ AND $M_{He} = 1.0 \times 10^{-2} M_*$

l, k	0.55 $M_\odot$ log g = 7.91 12,650 K	0.60 $M_\odot$ log g = 8.00 12,620 K	0.65 $M_\odot$ log g = 8.08 12,620 K	0.70 $M_\odot$ log g = 8.16 12,700 K	0.75 $M_\odot$ log g = 8.24 12,650 K	0.80 $M_\odot$ log g = 8.32 12,620 K	0.85 $M_\odot$ log g = 8.39 12,680 K	0.95 $M_\odot$ log g = 8.55 12,850 K
1, 1	163.4	152.1	141.3	131.7	123.2	115.3	107.8	92.8
1, 2	217.7	210.1	200.7	190.9	181.6	170.9	160.0	146.9
1, 3	283.5	269.9	253.5	236.5	220.7	205.2	190.0	160.3
1, 4	302.3	283.2	265.7	249.3	234.3	218.7	203.1	174.5
1, 5	364.5	347.4	329.5	310.5	292.7	274.0	255.2	219.8
1, 6	423.9	396.0	370.9	348.7	330.9	313.9	296.4	265.8
1, 7	470.8	458.2	439.2	413.5	387.3	361.5	336.6	296.1
1, 8	508.9	479.1	450.0	425.9	407.5	388.1	367.9	326.5
1, 9	552.9	522.3	494.0	466.8	442.1	416.3	389.6	340.2
1, 10.....	621.6	585.3	546.6	510.3	479.1	449.9	422.1	383.8
1, 11.....	656.2	626.9	596.6	563.7	531.3	497.2	463.1	410.2
1, 12.....	706.9	671.2	631.5	593.5	561.0	529.2	496.6	431.8
1, 13.....	745.9	706.2	669.1	631.6	596.7	560.1	522.6	454.5
1, 14.....	787.9	753.8	710.5	666.7	628.8	591.6	554.4	491.7
1, 15.....	831.8	784.9	744.4	704.9	668.4	628.4	587.7	524.4
2, 1	94.5	87.9	81.7	76.1	71.2	66.7	62.3	53.6
2, 2	128.8	124.5	119.2	113.6	108.4	102.3	96.1	89.3
2, 3	170.8	159.4	148.3	137.8	128.3	119.2	110.3	94.5
2, 4	183.0	174.5	165.2	155.3	145.9	136.0	125.9	105.0
2, 5	212.2	201.8	191.1	179.8	169.3	158.3	147.4	126.9
2, 6	245.3	229.1	214.6	201.7	191.4	181.6	171.4	153.5
2, 7	291.6	274.8	256.9	239.7	224.0	209.0	194.6	171.1

TABLE 6

PERIODS FOR LOW-OVERTONE MODES OF MODELS NEAR 11,700 K
$M_H = 5.0 \times 10^{-5} M_*$ AND $M_{He} = 1.0 \times 10^{-2} M_*$

l, k	0.55 $M_\odot$ log g = 7.91 11,750 K	0.60 $M_\odot$ log g = 8.00 11,750 K	0.65 $M_\odot$ log g = 8.08 11,780 K	0.70 $M_\odot$ log g = 8.16 11,610 K	0.75 $M_\odot$ log g = 8.24 11,690 K	0.80 $M_\odot$ log g = 8.32 11,530 K	0.85 $M_\odot$ log g = 8.39 11,530 K	0.95 $M_\odot$ log g = 8.55 11,590 K
1, 1	166.8	155.0	144.5	135.6	126.7	119.4	111.7	96.3
1, 2	226.4	217.6	207.8	198.4	187.0	176.8	165.5	151.7
1, 3	294.0	277.5	259.5	243.1	225.8	210.5	194.9	164.9
1, 4	309.8	290.7	273.3	258.0	240.8	225.5	209.3	180.7
1, 5	376.8	358.3	339.2	321.2	300.6	281.9	262.8	227.2
1, 6	434.0	405.7	381.3	362.6	343.3	327.3	310.1	276.6
1, 7	498.5	480.6	453.4	426.2	397.3	372.6	348.1	308.5
1, 8	523.6	493.4	469.2	453.5	430.8	414.0	396.0	351.2
1, 9	569.1	538.2	509.8	485.5	456.5	431.0	404.4	356.1
1, 10.....	640.3	598.9	559.5	526.5	493.3	466.8	439.8	398.5
1, 11.....	680.8	650.0	616.6	584.5	546.4	512.6	478.0	430.2
1, 12.....	732.2	691.0	650.2	617.6	581.7	551.6	518.8	451.7
1, 13.....	770.5	730.7	692.1	657.1	615.7	579.3	541.8	472.6
1, 14.....	822.3	779.1	732.0	692.5	650.2	614.4	576.9	508.9
1, 15.....	858.5	814.8	774.6	738.9	692.5	651.9	610.4	547.4
2, 1	96.4	89.6	83.5	78.4	73.2	69.0	64.5	55.7
2, 2	134.0	129.0	123.5	118.2	111.7	106.0	99.5	92.5
2, 3	174.8	162.7	151.3	141.3	131.1	122.2	113.1	97.2
2, 4	189.6	180.2	170.0	160.6	149.7	139.8	129.4	108.2
2, 5	219.1	207.9	196.5	185.8	173.7	162.9	151.8	131.2
2, 6	251.0	234.6	220.6	209.8	198.5	189.2	179.2	159.7
2, 7	300.0	281.2	262.7	246.4	229.6	215.3	201.2	178.2

dient become strong enough to "wash out" mode trapping by the other interfaces. In Table 13 we show the periods and oscillation kinetic energies for a 12,500 K 0.60 $M_\odot$ model with $M_H = 1.5 \times 10^{-4} M_*$; here we find trapped modes (kinetic energy minima) at k = 5, 8, 16, and 22. Of these, the trapped modes at $k = 8$ and 22 have the largest kinetic energy contrast, suggesting they might have the largest amplitudes.

The possibility of nearly every other mode being trapped by the hydrogen layer, along with the potential for weaker mode trapping at long periods, makes it difficult to explain why only a handful of independent modes are present in long period ZZ Ceti stars such as GD 154. One possibility is that the multiple chemical composition transition zones present in real ZZ Ceti stars have the right separation to create trapped modes with a stronger than normal resonance. Alternatively, the hydrogen layer mass of at least some ZZ Ceti stars is thinner than our model grid presently allows for. This would suggest that the common period pattern found by Clemens (1994) is either a coincidence or is due to a mixture of $l = 1$ and 2 modes. We suggest that the presence of only a few modes in the longer period stars is

TABLE 7

PERIODS FOR LOW-OVERTONE MODES OF MODELS NEAR 12,500 K
$M_H = 1.0 \times 10^{-5} M_*$ AND $M_{He} = 1.0 \times 10^{-2} M_*$

l, k	0.60 $M_\odot$ log g = 8.00 12,700 K	0.70 $M_\odot$ log g = 8.17 12,820 K	0.75 $M_\odot$ log g = 8.25 12,700 K	0.80 $M_\odot$ log g = 8.32 12,720 K	0.85 $M_\odot$ log g = 8.40 12,760 K	0.95 $M_\odot$ log g = 8.56 12,590 K	1.05 $M_\odot$ log g = 8.72 12,680 K
1, 1	177.5	153.1	142.3	132.9	123.8	107.1	91.4
1, 2	208.7	190.5	209.9	171.2	160.6	153.5	140.0
1, 3	271.9	244.9	226.2	217.0	202.1	180.1	153.3
1, 4	309.9	272.0	261.0	237.3	220.6	194.8	164.2
1, 5	344.7	311.0	337.7	286.8	274.2	253.8	212.9
1, 6	436.3	382.2	378.5	333.6	311.4	302.3	259.5
1, 7	460.0	421.3	396.8	385.8	365.8	327.8	289.4
1, 8	483.7	436.6	449.0	396.8	375.3	339.4	308.0
1, 9	559.8	488.9	477.8	428.6	402.0	388.9	329.3
1, 10.....	598.5	539.2	525.5	484.8	454.6	404.2	367.1
1, 11.....	651.8	583.1	566.8	516.0	484.5	441.6	381.8
1, 12.....	687.7	612.1	613.2	551.2	518.2	471.2	412.5
1, 13.....	732.2	657.5	632.2	582.0	544.3	502.3	439.7
1, 14.....	774.5	690.5	681.5	620.2	584.4	525.3	475.5
1, 15.....	810.5	726.8	715.6	654.2	615.2	561.0	486.9
2, 1	102.7	88.5	82.2	76.8	71.5	61.9	52.8
2, 2	123.5	113.3	125.3	102.5	96.5	97.8	87.4
2, 3	168.9	151.9	141.3	134.3	125.0	104.9	91.1
2, 4	182.1	159.2	151.0	138.4	128.3	112.7	95.7
2, 5	200.0	180.4	195.2	165.9	158.6	146.6	122.9
2, 6	253.1	220.9	219.3	192.8	179.9	174.5	149.9
2, 7	276.9	248.8	258.0	225.6	213.0	195.7	167.2

TABLE 8

PERIODS FOR LOW-OVERTONE MODES OF MODELS NEAR 11,700 K
$M_H = 1.0 \times 10^{-5} M_*$ AND $M_{He} = 1.0 \times 10^{-2} M_*$

l, k	0.60 $M_\odot$ log g = 8.00 11,830 K	0.70 $M_\odot$ log g = 8.17 11,750 K	0.75 $M_\odot$ log g = 8.25 11,610 K	0.80 $M_\odot$ log g = 8.32 11,640 K	0.85 $M_\odot$ log g = 8.40 11,750 K	0.95 $M_\odot$ log g = 8.56 11,670 K	1.05 $M_\odot$ log g = 8.72 11,460 K
1, 1	181.3	157.3	146.0	136.9	127.6	110.6	95.5
1, 2	216.3	198.3	224.6	177.4	165.3	156.5	126.9
1, 3	281.9	254.7	241.8	224.3	207.7	185.4	155.0
1, 4	317.9	279.8	268.0	243.9	226.1	199.9	165.4
1, 5	355.1	326.1	349.0	301.5	286.4	259.8	219.9
1, 6	448.2	393.7	393.8	344.5	321.6	312.2	269.8
1, 7	482.5	445.3	432.6	405.1	380.7	346.3	302.0
1, 8	500.7	461.3	462.4	420.9	399.7	351.2	321.7
1, 9	574.3	503.5	507.5	444.1	417.1	399.8	342.0
1, 10.....	618.3	562.6	545.2	502.4	468.5	421.9	378.9
1, 11.....	676.1	603.9	590.7	536.2	503.1	454.7	390.4
1, 12.....	708.1	640.7	645.0	574.8	538.0	486.0	430.7
1, 13.....	760.3	683.4	678.8	602.4	562.7	520.6	457.4
1, 14.....	804.0	722.4	711.6	647.3	606.4	544.7	479.1
1, 15.....	838.9	765.1	755.4	684.3	641.9	584.0	507.0
2, 1	104.8	90.9	84.3	79.1	73.7	63.8	55.2
2, 2	128.0	118.1	132.1	106.4	99.4	99.8	81.1
2, 3	174.7	157.5	152.4	138.4	128.2	107.7	89.8
2, 4	186.7	163.7	156.3	142.1	131.3	115.7	95.6
2, 5	206.1	188.9	201.6	174.4	165.5	150.0	126.9
2, 6	259.4	227.5	227.7	199.0	185.8	180.4	155.8
2, 7	285.1	259.8	266.6	235.0	220.4	201.2	174.4

probably due to the combination of mode trapping in a thick hydrogen layer white dwarf along with a driving region timescale that allows only the long-period modes to be unstable. Determining the mode structure and spectroscopic identification of the l values of the modes in other long-period ZZ Ceti stars will be critical for answering this question. If all of the long-period ZZ Ceti stars have only a few independent long-period modes present, it will suggest one of two things:

1. There is an interplay between mode trapping and the thermal timescale of the driving region which chooses long-period trapped modes.

2. The hypothesis of all ZZ Ceti stars having massive hydrogen layers requires revision.

Besides possibly explaining the paucity of observed modes in the long-period DAV stars, mode trapping may also provide an explanation for the period ratio of 1.54 seen between the dominant pulsation modes of several long-period DAV stars, such as BPM 31594, GD 154, and G29–38. In many models, the periods of the fourth- and second-order trapped modes have ratios close to 1.54, suggesting that mode trapping might be responsible. If mode trapping is the correct explanation, the hydrogen layer mass

TABLE 9

PERIODS FOR LOW-OVERTONE MODES OF MODELS NEAR 12,500 K
$M_H = 5.0 \times 10^{-6} M_*$ AND $M_{He} = 1.0 \times 10^{-2} M_*$

l, k	0.55 $M_\odot$ log g = 7.92 12,680 K	0.60 $M_\odot$ log g = 8.01 12,700 K	0.70 $M_\odot$ log g = 8.17 12,590 K	0.75 $M_\odot$ log g = 8.25 12,700 K	0.80 $M_\odot$ log g = 8.33 12,820 K	0.95 $M_\odot$ log g = 8.56 12,650 K	1.05 $M_\odot$ log g = 8.72 12,590 K
1, 1	201.8	189.1	164.9	152.2	141.7	113.7	97.2
1, 2	220.4	209.4	192.4	206.7	171.3	153.7	124.6
1, 3	283.3	271.2	247.1	224.5	217.2	182.8	154.9
1, 4	329.1	312.9	283.4	275.2	249.3	203.6	169.8
1, 5	383.7	356.1	316.2	341.6	285.3	267.1	225.5
1, 6	459.3	439.0	399.1	389.5	349.7	305.6	268.1
1, 7	482.2	463.9	429.3	397.0	385.9	329.3	297.8
1, 8	532.2	494.8	441.8	461.9	397.4	353.1	301.3
1, 9	593.0	564.4	510.3	485.9	445.5	396.9	346.0
1, 10.....	652.6	614.8	546.6	528.4	487.3	414.2	355.9
1, 11.....	685.2	651.1	598.1	581.2	530.1	445.8	388.1
1, 12.....	738.4	702.4	629.1	609.5	553.9	485.0	416.4
1, 13.....	783.9	739.2	667.9	651.2	594.8	506.8	444.5
1, 14.....	817.8	777.4	713.1	686.1	628.2	542.5	464.2
1, 15.....	880.1	831.1	740.7	718.8	660.4	566.1	502.9
2, 1	117.5	109.6	95.3	87.9	81.9	65.7	56.1
2, 2	129.2	123.6	114.4	124.6	102.5	98.0	79.7
2, 3	176.2	168.4	153.8	138.6	135.4	106.6	89.9
2, 4	194.5	184.6	165.3	159.0	144.4	117.6	98.1
2, 5	221.9	206.0	183.0	197.5	165.1	154.2	130.2
2, 6	269.2	255.7	231.0	226.4	202.1	176.6	154.8
2, 7	306.1	284.8	252.1	261.2	225.5	203.7	173.4

TABLE 10

PERIODS FOR LOW-OVERTONE MODES OF MODELS NEAR 11,700 K
$M_H = 5.0 \times 10^{-6} M_*$ AND $M_{He} = 1.0 \times 10^{-2} M_*$

l, k	0.55 $M_\odot$ log g = 7.93 11,800 K	0.60 $M_\odot$ log g = 8.01 11,860 K	0.70 $M_\odot$ log g = 8.17 11,800 K	0.75 $M_\odot$ log g = 8.25 11,610 K	0.80 $M_\odot$ log g = 8.33 11,690 K	0.95 $M_\odot$ log g = 8.56 11,690 K	1.05 $M_\odot$ log g = 8.72 11,670 K
1, 1	207.5	193.4	168.0	156.3	145.9	116.8	100.1
1, 2	226.8	216.5	198.0	215.2	177.5	156.7	126.5
1, 3	294.3	281.2	254.4	235.1	224.5	189.0	159.3
1, 4	339.2	322.7	290.9	282.3	257.1	208.1	173.2
1, 5	391.8	364.4	325.8	356.0	300.5	274.0	230.7
1, 6	476.6	454.2	409.8	403.8	361.0	316.9	277.1
1, 7	506.6	487.8	445.5	424.1	406.3	350.0	308.3
1, 8	543.6	506.9	460.3	481.8	422.9	362.0	317.7
1, 9	613.3	583.3	523.2	509.7	459.4	413.1	355.2
1, 10.....	673.0	630.9	562.6	551.4	508.7	428.0	373.8
1, 11.....	708.7	676.6	618.0	599.9	549.4	460.9	400.4
1, 12.....	766.0	726.1	646.7	644.6	577.8	498.3	429.3
1, 13.....	811.2	763.6	690.6	678.0	619.0	528.4	461.3
1, 14.....	858.9	811.2	737.8	720.1	654.0	559.7	480.2
1, 15.....	909.8	857.8	768.0	755.0	698.1	595.4	519.1
2, 1	120.6	111.9	97.1	90.2	84.3	67.5	57.8
2, 2	133.2	128.0	117.9	130.9	106.4	100.0	80.9
2, 3	182.6	174.4	158.4	143.5	139.6	109.9	92.4
2, 4	200.4	189.9	169.2	163.0	148.7	120.2	100.0
2, 5	226.6	210.8	188.6	205.7	173.8	158.2	133.2
2, 6	277.4	263.6	237.0	233.5	208.6	183.1	160.0
2, 7	312.8	291.2	259.4	275.9	236.0	208.7	178.2

of these stars must be greater than $10^{-5} M_*$ for the fourth trapped mode to have a period near 615 s that we see for several ZZ Ceti stars.

Although the three observed periods are too few for a meaningful period spacing diagram, G117-B15A shows mode trapping effects. If we assume all three modes (at 215.2, 270.4, and 304.0 s) are $l = 1$ modes, we could explain the relatively small spacing between the 270 and 304 s periods as the result of the 270 s mode being trapped, which our models with $M_H \sim 10^4 M_*$ predict.

4.2. *Effects of Other Composition Transition Zones*

Our models have thick enough hydrogen layers that the He/C and C/O composition gradients can significantly modify the mode-trapping resonances of the hydrogen layer, especially for low-overtone modes. Models used to duplicate the periods of G117-B15A illustrate this effect: a pure carbon core model has periods of 216, 270, and 319 s, whereas a model with a 20:80 C/O core out to $0.75 M_*$ has periods of 212, 271, and 304 s. In this example, additional

TABLE 11

PERIODS FOR LOW-OVERTONE MODES OF MODELS NEAR 12,500 K
$M_H = 1.0 \times 10^{-6} M_*$ AND $M_{He} = 1.0 \times 10^{-2} M_*$

l, k	0.55 $M_\odot$ log g = 7.93 12,560 K	0.60 $M_\odot$ log g = 8.02 12,360 K	0.65 $M_\odot$ log g = 8.10 12,790 K	0.70 $M_\odot$ log g = 8.18 12,620 K	0.80 $M_\odot$ log g = 8.33 12,390 K	0.95 $M_\odot$ log g = 8.56 12,470 K	1.05 $M_\odot$ log g = 8.73 12,680 K
1, 1	211.4	204.3	193.2	186.5	167.1	133.2	111.7
1, 2	246.0	230.6	212.5	198.9	174.0	154.9	124.9
1, 3	284.4	274.3	257.2	246.0	219.3	183.4	158.6
1, 4	326.9	312.7	294.0	283.8	265.1	232.5	194.8
1, 5	425.7	402.1	372.5	350.0	307.3	279.1	246.9
1, 6	465.2	443.1	414.5	398.0	367.5	329.5	278.9
1, 7	484.2	473.6	446.2	434.1	403.4	337.7	301.5
1, 8	560.3	536.1	501.1	476.3	421.0	382.8	330.1
1, 9	621.3	584.3	541.5	513.4	466.8	411.3	354.0
1, 10.....	658.3	635.5	597.9	575.7	520.6	428.7	367.6
1, 11.....	713.4	686.3	642.4	611.9	546.7	479.4	406.2
1, 12.....	765.5	724.7	673.6	641.9	583.1	504.2	433.9
1, 13.....	796.3	768.0	721.0	694.5	625.8	534.8	461.5
1, 14.....	848.9	815.3	763.2	729.6	659.5	571.0	488.3
1, 15.....	914.8	864.3	801.2	760.9	690.8	587.3	521.8
2, 1	124.6	120.4	113.9	109.6	97.1	76.9	64.5
2, 2	142.6	133.8	123.4	116.1	103.4	98.6	80.0
2, 3	175.6	169.4	159.4	153.0	136.8	107.0	92.0
2, 4	194.4	185.5	173.6	166.2	153.6	134.2	112.5
2, 5	246.6	232.6	215.3	202.3	177.5	161.2	142.6
2, 6	271.0	257.1	240.4	230.6	212.7	190.4	161.1
2, 7	318.6	307.1	287.8	274.2	242.6	219.8	189.6

TABLE 12

PERIODS FOR LOW-OVERTONE MODES OF MODELS NEAR 11,700 K
$M_H = 1.0 \times 10^{-6} M_*$ AND $M_{He} = 1.0 \times 10^{-2} M_*$

l, k	0.55 $M_\odot$ log g = 7.93 11,910 K	0.60 $M_\odot$ log g = 8.02 11,690 K	0.65 $M_\odot$ log g = 8.10 11,940 K	0.70 $M_\odot$ log g = 8.18 11,800 K	0.80 $M_\odot$ log g = 8.33 11,860 K	0.95 $M_\odot$ log g = 8.56 11,690 K	1.05 $M_\odot$ log g = 8.73 11,590 K
1, 1.....	217.6	210.8	200.3	191.9	170.1	135.9	115.4
1, 2.....	249.4	234.7	216.7	202.7	177.0	157.4	121.2
1, 3.....	292.6	282.3	266.0	253.3	223.0	188.7	164.1
1, 4.....	334.5	321.2	304.1	293.5	272.1	237.2	199.9
1, 5.....	434.3	410.2	381.1	357.6	312.8	289.1	258.0
1, 6.....	475.5	454.2	428.0	411.2	376.7	336.7	289.2
1, 7.....	503.5	494.6	469.9	456.0	417.1	424.8	317.7
1, 8.....	574.1	549.6	515.8	487.9	428.3	441.3	341.4
1, 9.....	632.7	596.3	555.7	528.1	477.7	491.3	370.4
1, 10.....	677.4	655.4	620.2	594.7	530.4	519.7	380.9
1, 11.....	734.4	706.8	663.4	628.7	558.3	553.2	418.6
1, 12.....	782.9	742.8	694.8	663.1	596.2	588.5	451.0
1, 13.....	820.5	794.7	750.8	719.3	638.2	614.5	479.5
1, 14.....	873.1	842.0	792.4	755.0	676.3	643.1	509.5
1, 15.....	936.0	888.6	827.3	787.1	709.8	683.4	550.3
2, 1.....	128.2	124.2	117.9	112.5	98.8	78.5	66.6
2, 2.....	144.6	136.2	126.1	118.7	105.4	100.3	77.6
2, 3.....	180.3	174.3	164.8	157.7	139.0	109.9	95.1
2, 4.....	199.0	190.2	179.0	171.3	157.5	136.9	115.4
2, 5.....	251.4	237.2	220.2	206.6	180.7	167.0	149.0
2, 6.....	276.0	263.2	247.9	238.1	218.0	194.5	167.1
2, 7.....	327.9	315.4	296.6	281.0	246.5	226.9	193.9

mode trapping by the C/O gradient is responsible for bringing the 319 s period down closer to the observed 304 s. With this in mind, we examine in more detail the effects of the He/C and C/O composition gradients on mode trapping.

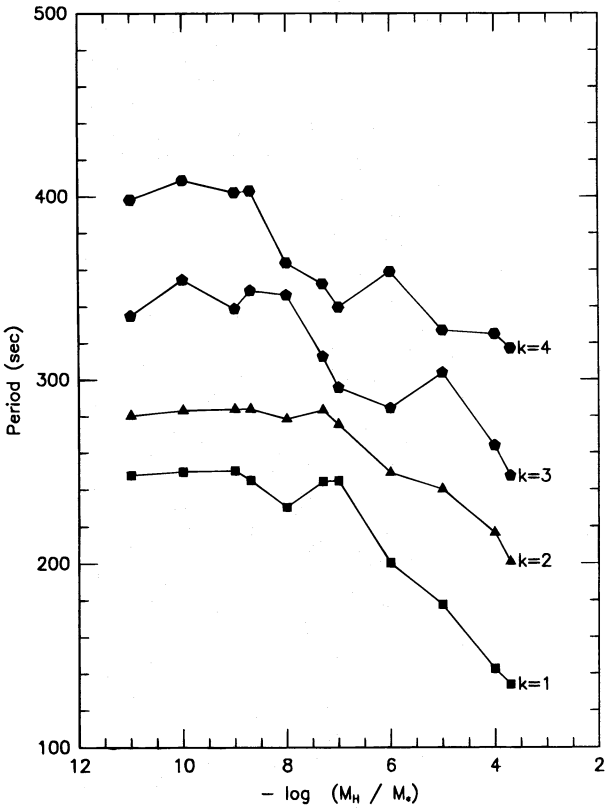

FIG. 4.—Periods of the first four overtone $l = 1$ modes from 0.60 $M_\odot$ models with different hydrogen layer masses. The consecutive overtone modes have similar periods (closely spaced vertically) when a mode is trapped. Here the $k = 2$ mode is trapped near $M_H = 10^{-7} M_*$, and the $k = 3$ mode is trapped when $M_H \approx \approx 10^{-5} M_*$ or $10^{-8} M_*$.

We start by examining the He/C gradient for carbon core models with hydrogen layers of $10^{-10} M_*$ and $1.5 \times 10^{-4} M_*$. When $M_H = 10^{-10} M_*$, we vary the helium layer mass between $10^{-2} M_*$ and $10^{-8} M_*$, and we see noticeable differences in the pulsation periods at $k = 1$ and $k \gtrsim 8$ (see Fig. 5). When $M_{He} = 10^{-2} M_*$, the helium layer traps the $k = 1$ mode, causing its period to be about 210 s instead of about 250 s as seen in the other models. We see this in the eigenfunctions (see Fig. 6) for the $k = 1$ mode; it penetrates down to $10^{-2} M_*$ when $M_{He} = 10^{-2} M_*$, but only to $\sim 10^{-4} M_*$ when the helium layer mass is $10^{-4} M_*$ or less). This outward displacement of the eigenfunction is responsible for lengthening the period of the $k = 1$ mode as the helium layer mass drops. Our models with $M_{He} = 10^{-8} M_*$ have the most trapped mode at $k = 9$ instead of $k = 8$, because of differences in the interaction between the He/C and H/He composition transition zones on mode trapping. There is also a general increase in the pulsation periods of models as the helium layer mass thickens, seen especially at longer periods. The period increase is the result of the faster cooling histories of models with (more transparent) thick helium layers. When the hydrogen layer mass is $1.5 \times 10^{-4} M_*$, we are physically limited to examining models with helium layers between $M_{He} = 1.5 \times 10^{-2} M_*$ and $2.5 \times 10^{-2} M_*$. Here the helium layer masses are so similar that there is very little difference in the periods. Also, if the hydrogen layer is $\sim 10^{-4} M_*$, we have significant indirect constraints on the helium layer mass from physical self-consistency requirements. In this case, diffusion and the lack of helium burning would fix the helium layer mass somewhere between about $10^{-2} M_*$ and $2 \times 10^{-2} M_*$. This limit is a significant improvement compared to the helium layer mass range of $10^{-2} M_*$ to $\sim 10^{-8} M_*$ that we had before.

Next, we look at the effect of changing the steepness of the H/He and He/C gradients, while leaving the midpoint at the same mass point in the model. At the H/He transition zone, the thickness can be modified by diffusion-fed *p-p*

TABLE 13

PERIODS AND OSCILLATION KINETIC ENERGIES FOR A 0.60 $M_\odot$ MODEL NEAR 12,500 K $M_H = 1.5 \times 10^{-4} M_*$ AND $M_{He} = 1.5 \times 10^{-2} M_*$

l, k	Period (s)	log Kinetic Energy
1, 1	136.8	50.95
1, 2	204.0	49.71
1, 3	251.6	49.06
1, 4	283.6	48.31
1, 5	333.6	48.05 T
1, 6	376.3	48.26
1, 7	441.8	48.08
1, 8	466.3	46.87 T
1, 9	507.6	47.63
1, 10.....	550.0	47.87
1, 11.....	609.9	47.66
1, 12.....	652.1	46.90
1, 13.....	689.5	46.66
1, 14.....	726.0	46.53
1, 15.....	769.7	46.40
1, 16.....	804.2	46.35 T
1, 17.....	850.9	46.58
1, 18.....	893.8	46.54
1, 19.....	942.7	46.52
1, 20.....	986.5	46.12
1, 21.....	1027.1	46.01
1, 22.....	1066.7	45.65 T
1, 23.....	1102.0	45.90
1, 24.....	1145.5	46.18
1, 25.....	1194.3	46.41
1, 26.....	1247.1	46.12
1, 27.....	1290.2	45.64

NOTE.—The kinetic energy values have the units of ergs, with the normalization of $\delta r/r = 1$ at the surface of the model for each eigenmode. A "T" in column (3) indicates a trapped mode.

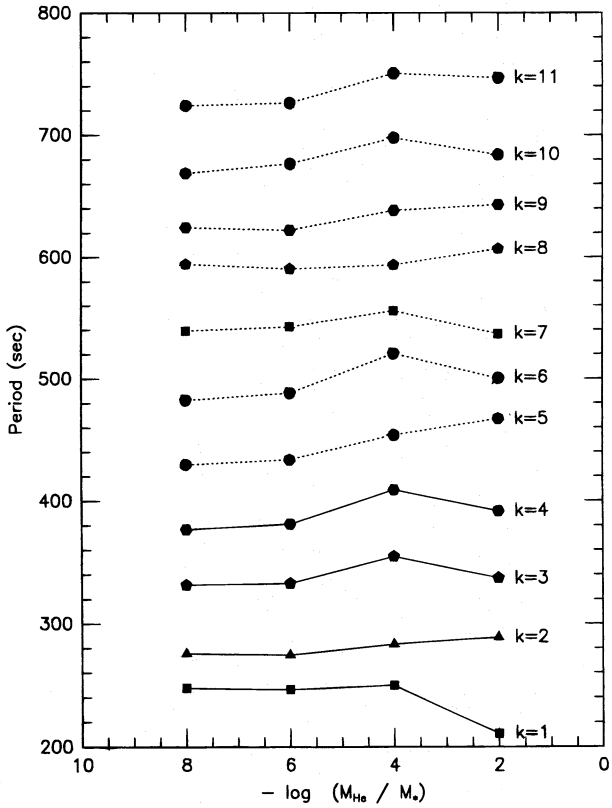

FIG. 5.—Periods of low-overtone $l = 1$ modes for models with $M_H = 10^{-10} M_*$ and several different helium layer masses. Note especially the difference in the period spacing between the $k = 1$ to 2, 4 to 5, and 7 to 8 modes when $M_{He} = 10^{-2} M_*$ and models that have thinner helium layers. These differences are due to additional mode trapping by the deep He/C interface.

burning. The He/C transition zone may be different because of the interplay between diffusion and degeneracy in addition to the possibility of the profile starting out differently than we have specified. As we demonstrate, the period changes are fairly subtle. We will need to detect most or all of the low-overtone modes in order to constrain the extent of the transition zones. Attempting to observe these modes is worthwhile, because doing so would offer us the chance to determine the extent of the transition zones and the processes that determine their thickness.

The following examples provide a sample of what to expect when we change the transition zone extent in our models. Reducing the He/C composition gradient thickness from 2.0 to 1.5 pressure scale heights (PSH) decreases the $k = 2$ mode period by up to 10 s in the models we examine, while all the other modes change by less than 4 s. Making the H/He composition gradient steeper (0.52 to 0.45 PSH) reduces the period of the $k = 1$ mode up to 6 s and decreases the period of the $k = 3$ and 5 modes by as much as 8 s. A steeper H/He composition gradient also *raises* the period of the $k = 6$ mode by up to 10 s. As we mentioned earlier, these changes are small enough that we need to have periods for all of the low-overtone modes; it will also be important to know that we have the $m = 0$ periods, as m ambiguity can mimic transition zone changes.

Next, we explore changes in the core composition using 0.55 $M_\odot$ models with $M_H = 1.5 \times 10^{-4} M_*$ and $M_{He} = 1.5 \times 10^{-2} M_*$ in our examples. We expect to see mode-trapping changes only at low overtones, because these are the modes with the largest core amplitudes. We also expect a general lengthening of our predicted periods for high-overtone modes ($k \gtrsim 10$) as the core becomes oxygen-rich. The period lengthening is the result of oxygen core models being older and having more degenerate cores at a given effective temperature.

First, we change the composition of the core from pure carbon to pure oxygen. In these models, we use a uniform C/O mass ratio out to $0.80 M_*$, and change the composition to pure carbon by $0.90 M_*$. Most of the period shifts we see result from the increasingly steep composition gradient, causing stronger mode trapping. Because these structural changes occur in the core, we see the most significant period shifts in low-overtone modes (see Fig. 7), because they have the largest core amplitudes. The $k = 2$ mode drops by up to 10 s as the oxygen mass fraction increases. However, the most dramatic changes occur at $k = 4$ and $k = 8$—these modes drop by up to 30 and 20 s, respectively, as the oxygen fraction increases. Other modes experience period shifts of less than 5 s.

In our last experiment, we keep the core composition constant at 20:80 C/O and fix the outer transition point at $0.90 M_*$, while we vary the location of the inner transition point between $0.50 M_*$ and $0.85 M_*$. As we move the inner C/O transition point outward, we steepen the composition gradient and increase the mode-trapping effectiveness of the C/O interface. Moving the inner C/O transition point causes the strongly trapped mode to shift from $k = 4$ when the transition point is at $0.50 M_*$ to $k = 3$ at $0.60 M_*$ or

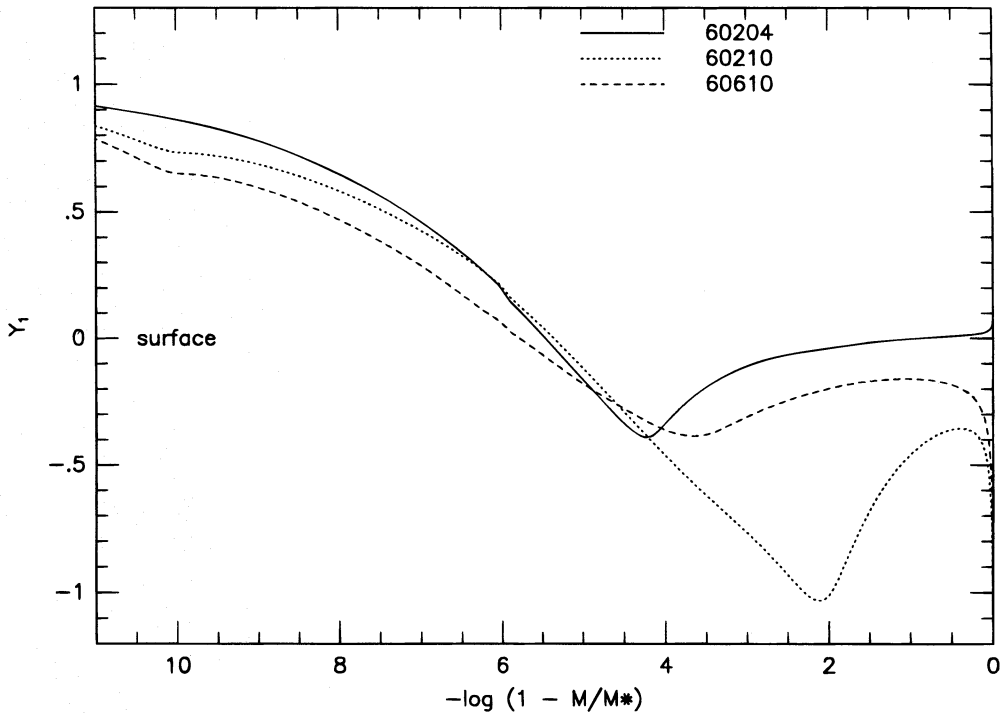

FIG. 6.—$\delta r/r$ eigenfunctions for $l = 1$, $k = 1$ modes of models with $M_H = 10^{-10}M_*$ and $M_{He} = 10^{-2}M_*$ (*short-dashed line*) and $M_{He} = 10^{-6}M_*$ (*long-dashed line*). The eigenfunction has a much lower core amplitude when $M_{He} = 10^{-6}M_*$, causing the period to be longer. For comparison, we also plot the same eigenfunction for a model with $M_H = 10^{-4}M_*$ and $M_{He} = 10^{-2}M_*$ (*solid line*).

more. As the inner transition point moves farther out, the kinetic energy contrast between the $k = 3$ and 4 modes increases, and the $k = 4$ mode period increases by 35 s as a result (see Fig. 8). The periods of the $k = 7$ and 8 modes

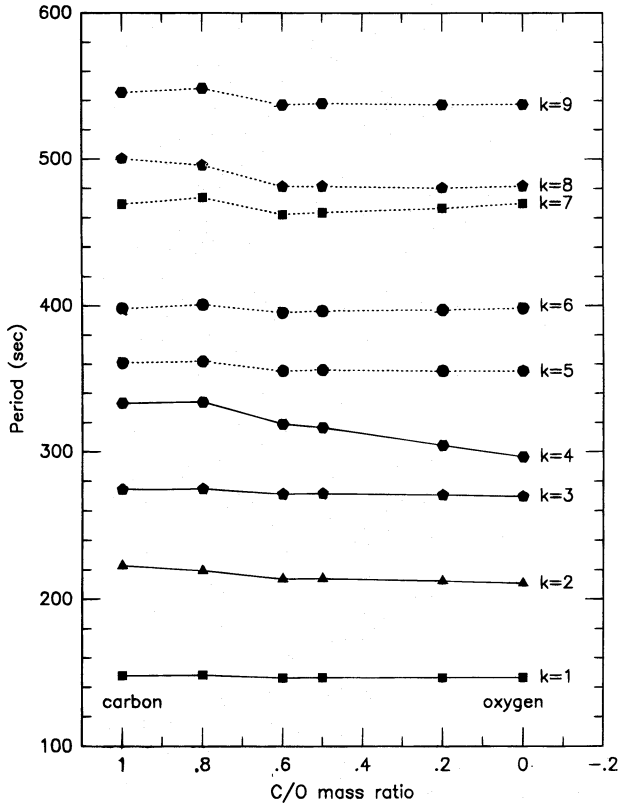

FIG. 7.—Periods of low-overtone $l = 1$ modes for cores with different C/O mass fractions (0.60 $M_\odot$ models). Note the large change in the $k = 4$ mode period in response to the changing C/O mass fraction. The $k = 7$ and 8 mode periods show smaller changes.

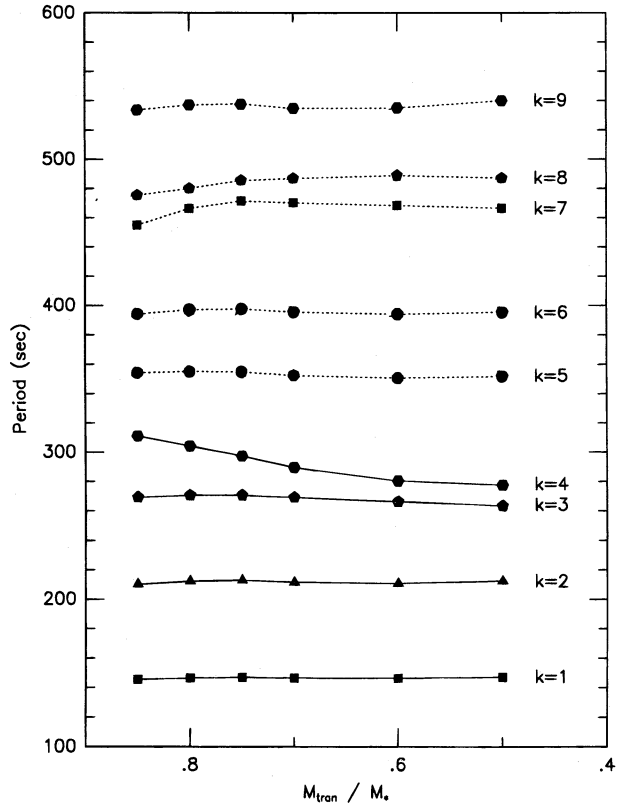

FIG. 8.—Periods of low-overtone $l = 1$ modes for models with 20:80 C/O cores that have different inner transition point locations (0.60 $M_\odot$ models). The $k = 4$ mode period increases by about 25 s as the transition point moves outward in the model. The most trapped mode changes from $k = 4$ to $k = 3$ as the C/O transition point moves outward, causing the large period increase. The $k = 7$ and 8 mode periods show smaller changes for the same reason.

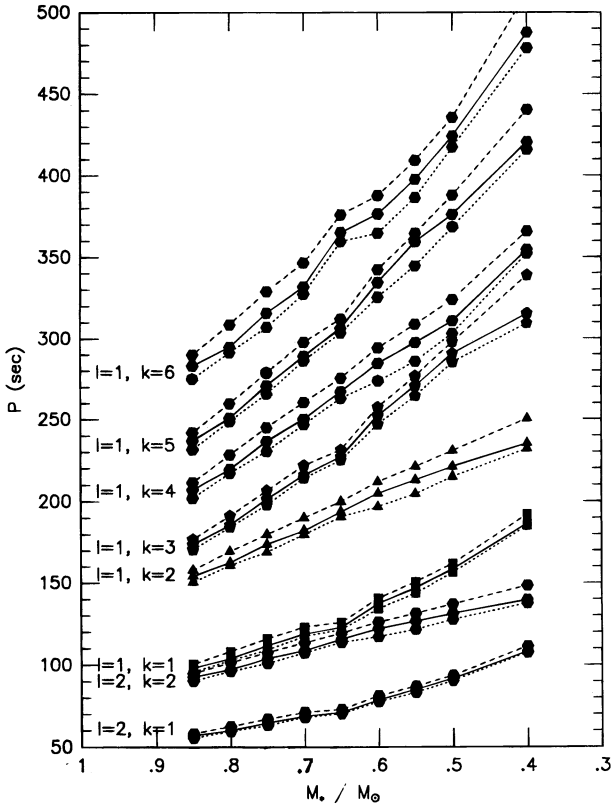

FIG. 9.—Periods of low-overtone $l = 1$ and 2 modes in DA models with $M_{He} = 10^{-2}M_*$, $M_H = 1.5 \times 10^{-4}M_*$, at three different effective temperatures. The upper (*dashed*) lines correspond to ~11,500 K model periods, the middle (*solid*) lines correspond to ~12,500 K model periods, and the lower (*dotted*) lines correspond to ~13,200 K model periods. The periods increase with decreasing effective temperature because the core becomes increasingly degenerate.

drop slightly when the inner C/O transition point is closest to the surface, suggesting that they "feel" the interface near $0.8M_*$. Modes with $k \geq 11$ have longer periods as the transition point moves out, because the increasing amount of oxygen in the core speeds evolutionary cooling.

In summary, changing the steepness and location of the He/C and C/O interfaces affects the periods of low-overtone modes the most. Also, most of the effects are subtle enough that we will need observational detections of almost all the low-overtone modes, along with accurate m identifications. A sharper H/He interface shortens the $k = 1$, 3, and 5 mode periods, while increasing the $k = 6$ mode period, whereas a sharper He/C interface decreases only the $k = 2$ mode period. Changes in the core C/O mass fraction and location of the C/O inner transition point affect the $k = 4$ and $k = 7$ to 8 modes the most; their periods can change by as much as 20–30 s.

In § 6 we demonstrate that the observed period structure of G117-B15A shows clear signs of an extra interface, which we attribute to the C/O core. Only when we use a model with a 20:80 C/O core and an inner C/O transition point near $0.80M_*$ are we able to duplicate the periods at 270 and 304 s with $l = 1$ modes.

4.3. *Effects of Stellar Mass*

Changing the stellar mass has a dramatic effect on the theoretical pulsation periods of our models, but the effect is different from changes caused by mode trapping. Increasing the stellar mass decreases the periods and period spacings of *all* modes, rather than only the period of the $k = 1$ mode, as shown in Figure 9 for $M_H = 1.5 \times 10^{-4}M_*$. The pulsation periods vary as the inverse of the Brunt-Väisälä frequency because of the increase in the Brunt-Väisälä frequency in the outer layers of a more massive model.

If we consider G117-B15A, the 215 s mode can be an $l = 1$, $k = 2$ mode for models near 0.55 $M_\odot$ or the $l = 1$, $k = 3$ mode for 0.7 $M_\odot$ models. (We can rule out the 215 s mode being $k = 1$ when $M_H = 1.5 \times 10^{-4}M_*$, because even our 0.40 $M_\odot$ models have periods of only 185 s.) We can eliminate this ambiguity by considering the 270 and 304 s modes as well; including these modes in our fit clearly favors 0.55 $M_\odot$ models.

5. EVOLUTIONARY EFFECTS ON WHITE DWARF PULSATIONS

5.1. *Pulsation Periods*

All white dwarfs cool as they age, causing the Brunt-Väisälä frequency to decrease, and causing the pulsation periods to lengthen in response. Short-period modes do not increase much as a model cools through the instability strip—typically less than 15 s for $l = 1$ modes with periods less than 300 s. This period change due to evolutionary cooling is considerably less than the ~50 s between consecutive overtone modes, so there is relatively little chance for an incorrect mode assignment for a given l here. Longer period modes lengthen more as our models cool, because their eigenfunctions are concentrated closest to the surface where structural changes are the greatest. At around $k = 13$ (680 s in 0.60 $M_\odot$ models), the period shift as a model cools through the instability strip is about 50 s, comparable to the period spacing between consecutive overtone modes. As an example of the confusion we face, consider an $l = 1$, 615 s mode (seen in several stars), and let us assume that the hydrogen layer mass is $1.5 \times 10^{-4}M_*$. We could identify this as the $k = 15$ (11,700 K) or 16 (13,200 K) mode of a 0.80 $M_\odot$ model, the $k = 13$ mode of a 12,300 K 0.70 $M_\odot$ model, or the $k = 11$ mode of a 12,080 K 0.60 $M_\odot$ model. We require extra constraints to make a unique mode assignment, such as demanding the 615 s mode be a trapped mode and that the effective temperature be about 12,000 K. With these additional constraints, we can then identify it as the $k = 11$ mode of a 0.60 $M_\odot$ model. We did not need to use the spectroscopic log g to determine the mass, so comparing the spectroscopic and seismological log g values gives us an independent confirmation of our seismology.

5.2. *Rates of Period Change*

If we consider how fast the period of a given mode changes with time, we have the rate of period change, denoted by dP/dt or $\dot{P}$. Typical theoretical evolutionary values of $\dot{P}$ range from 10^{-14} to 10^{-15} s s^{-1}, and the value is more sensitive to changes in the stellar mass and core composition than anything else. Bradley et al. (1992) present dP/dt values for 0.5 and 0.6 $M_\odot$ models with carbon and oxygen cores, so here we only cover variations in hydrogen layer mass and stellar mass.

Besides measuring the cooling timescale of a white dwarf, the small dP/dt values for evolutionary cooling predicted by our models mean their eventual detection will also impose strong constraints on the presence of other mechanisms that can change the pulsation period. For instance, changes in the rotation rate, magnetic field strength, nonlinear mode

coupling, and binary orbital motion can change the pulsation period, and all operate on timescales shorter than typical evolutionary cooling timescales. Given the possible presence of any or all of these mechanisms in real stars, the upper limit on dP/dt for G117-B15A of $(1.2 \pm 2.9) \times 10^{-15}$ s s^{-1} (Kepler et al. 1995) for the dominant pulsation mode at 215.2 s suggests that nothing affects this pulsation mode on timescales of less than $\sim 10^9$ yr, to within 3 σ. However, the 215.2 s mode is a low-overtone mode, and we least expect it to be influenced by processes operating close to the surface, such as mode coupling or a dynamo-generated magnetic field. We will place better constraints on the presence of period change mechanisms when we constrain the rate of period change of the other two pulsation modes. Thus, we do not have to wait to *detect* a rate of period change to say something significant about pulsations in white dwarfs, such as the absence of a binary companion or short term changes in the driving region properties.

The hydrogen layer mass affects dP/dt through mode trapping; trapped modes are concentrated closer to the surface, where residual gravitational contraction is still appreciable. Contraction acts to *reduce* the pulsation period and counteract the period increase due to evolutionary cooling, causing trapped modes to have smaller rates of period change. Typically, it is 20%–30% less than dP/dt for nontrapped modes.

We find a much larger variation in the rate of period change when we consider the stellar mass. Here there is more than a factor of 4 change in dP/dt between the 0.4 and 0.8 $M_\odot$ models (see Table 14), while Bradley et al. (1992) show only a 20% change in dP/dt between carbon and oxygen cores for a given mass. Because the rate of period change is so much more sensitive to the stellar mass than anything else, a large dP/dt value will suggest the star is less massive than average. The decades-long timescales required to obtain a 20%–30% accuracy for dP/dt values will make it difficult for us to obtain rates of period change for mode trapping or C/O core composition diagnostics. Thus, performing asteroseismology using pulsation periods will give us accurate mass values more quickly than rates of period change. Rates of period change will still be useful as an independent means of confirming the seismological inferences made by other means.

Our models predict that DAV stars with masses greater than $\sim 0.90\ M_\odot$ will be crystallizing in the core as they cool through the instability strip. When this happens, dP/dt will be even lower than predicted by extrapolating values from lower mass models, because core cooling is temporarily slowed by the release of the latent heat of crystallization. BPM 37093 may offer us the opportunity to measure dP/dt for a white dwarf with a crystallizing core. Bergeron et al. (1995) derive a spectroscopic mass between 1 and 1.1 $M_\odot$ for BPM 37093, consistent with the earlier log g determinations of Bragaglia, Renzini, & Bergeron (1993) and Koester & Allard (1993). Our models show that modes near the observed quasiperiod of 600 s have dP/dt values between (2–3) $\times 10^{-15}$ s s^{-1}, about half of what we would expect if the core were not crystallizing. Iben (1991) suggests that a 1.1 $M_\odot$ white dwarf would have an O/Ne/Mg core, which at these temperatures would be fully crystallized. In this case, dP/dt could be several times larger than our estimate because of Debye cooling.

6. AN EXAMPLE: SEISMOLOGY OF G117-B15A

In this section we demonstrate our procedures for the asteroseismology of short-period DAV stars using G117-B15A as an example. G117-B15A has three modes—at 215, 270, and 304 s (Kepler et al. 1982)—which is typical of the hotter—and simpler—DAV stars. Robinson et al. (1995) positively identify the 215 s period as an $l = 1$ pulsation mode, but they could not determine the l value of the other two modes. Clemens (1994) interprets the three periods as the $k = 2$, 3, and 4, $l = 1$ modes, although Fontaine et al. (1994) identify them as $k = 1$, 2, and 3. G117-B15A also has the best upper limit to dP/dt of any DA white dwarf, with the latest value being $(1.2 \pm 2.9) \times 10^{-15}$ s s^{-1} (Kepler et al. 1995), containing data through 1995 March. There is considerable spread in both the observed effective temperature

TABLE 14

RATES OF PERIOD CHANGE FOR SELECTED MODES: 0.4–1.05 $M_\odot$

l	k	c40410 12,830 K 2.45×10^8 yr $\dot{P}$	c50410 13,020 K 3.08×10^8 yr $\dot{P}$	c60410 12,870 K 4.21×10^8 yr $\dot{P}$	c70410 13,080 K 5.21×10^8 yr $\dot{P}$	c80410 12,880 K 6.94×10^8 yr $\dot{P}$	c950610 13,090 K 10.32×10^8 yr $\dot{P}$	c105610 13,040 K 13.65×10^8 yr $\dot{P}$
1.....	1	8.44	7.09	2.19	1.80	2.07	1.89	0.75
1.....	2	6.12	5.40	6.08	5.34	3.97	1.88	1.56
1.....	3	8.57	8.79	7.64	4.32	2.28	2.44	2.04
1.....	4	12.66	10.96	5.14	7.08	5.27	3.00	0.87(T)
1.....	5	13.77	7.17	7.94	7.08	3.06	1.63(T)	2.26
1.....	6	9.46	12.66	7.72	4.59	5.29	3.50	1.74
2.....	1	4.25	3.34	1.15	1.03	1.19	0.93	0.41
2.....	2	3.72	3.99	4.17	3.60	2.35	1.45	1.05
2.....	3	5.97	5.79	4.11	1.75	1.62	1.43	0.57(T)
2.....	4	7.85	5.79	3.04	4.16	3.14	1.84	1.13
2.....	5	6.60	4.74	5.20	2.83	1.70	0.81(T)	1.24
2.....	6	7.24	8.07	3.64	3.89	2.08(T)	2.15	0.99(T)
2.....	7	10.87	4.72	5.08	2.55(T)	3.42	1.41(T)	1.64
2.....	8	7.31	8.11	3.70(T)	4.32	2.73(T)	2.53	1.54
2.....	9	10.72	7.13(T)	5.62	4.24	4.27	2.58	1.27
2.....	10	8.05(T)	10.40	5.90	5.11	3.56	2.19	1.53
2.....	11	10.47	9.00(T)	7.05	5.49	4.85	2.78	1.42(T)
2.....	12	12.10	11.82	7.13	5.64	4.26	2.29(T)	2.35

NOTE.—All $\dot{P}$ values are in units of 10^{-15} s s^{-1}. A "(T)" after a $\dot{P}$ value indicates a trapped mode.

and log g values, although most of the recent studies give values near 12,400 K (Robinson et al. 1995; Koester, Allard, & Vauclair 1994). Bergeron et al. (1995) derive a temperature of 11,600 K, but they use less efficient convection. When the treatment of convection is consistent, they derive similar effective temperatures. The most recent published gravities range from 7.97 (Bergeron et al. 1995) to 8.12 (Koester et al. 1994). We start by using $\sim$12,400 K as the effective temperature and try masses near 0.60 $M_\odot$ (log $g \sim 8$) for models in our analysis.

Before we start looking at detailed model fits, we note that Robinson's (1995) determination of the 215 s mode being $l = 1$ immediately places a lower limit of $\sim 10^{-6} M_*$ on the hydrogen layer mass when the stellar mass is $\sim$0.6 $M_\odot$ when we assume it is the $k = 1$ mode. This hydrogen layer mass is consistent with the value quoted by Fontaine et al. (1994). If we assume the 215 s mode is $k = 2$, then the hydrogen layer mass must be close to $10^{-4} M_*$. These hydrogen layer mass limits *do not* depend on the details of the model structure but are set by the identification of the 215 s mode as an $l = 1$ mode. In what folows, we take the extra step to try and fit specific models to all three observed periods.

We start by looking for 215 s modes with $k = 2$, and our 0.55 $M_\odot$ models match this when $T_{\rm eff} \sim$ 12,000 K and the hydrogen layer mass is near $10^{-4} M_*$. Then, if we try to fit the 270 and 304 s modes, we immediately eliminate carbon core models, because they cannot match both the 270 and 304 s modes (see Table 15). We can match all three modes at once with models that have 20:80 C/O cores extending to between $0.75 M_*$ and $0.80 M_*$, a linear change to pure carbon by $0.90 M_*$, and a hydrogen layer mass of $1.5 \times 10^{-4} M_*$ (see Table 16). Changing the core composition from 20:80 C/O, moving the C/O gradient, or changing the hydrogen layer mass all make the $k = 4$ mode period deviate unacceptably from 304 s. Thus, if we accept the mode identification for G117-B15A, then we have a well-constrained fit for a 0.55 $M_\odot$ model at $\sim$12,300 K, consistent with the temperature derived by Robinson et al. (1995) and Koester et al. (1994). Our seismological temperature is high compared to what Bergeron et al. (1995) derive. Our experience shows we can fix this by slightly increasing the mass of the model (to 0.56 or 0.57 $M_\odot$) or by adjusting the convective efficiency of the model atmosphere used in spectroscopy. The surface gravity of the 0.55 $M_\odot$ model is 7.90, matching the value of Brassard et al. (1993), but is a little more than 1 σ below the value of Koester et al. (1994) and Bergeron et al. (1995). We can use the luminosity of our best model, along with a suitable bolometric correction and the observed visual magnitude, to predict a seismological parallax (see Bradley & Winget 1994b for details). Our predicted parallax of 15.9 milliarcseconds (mas) is higher than the observed value of 10.5 ± 4.2 mas (van Altena, Lee, & Hoffleit 1994), but this comparison is not very significant—yet.

Fontaine et al. (1994) mention a hydrogen layer mass of $1.2 \times 10^{-6} M_*$ for G117-B15A, which we can duplicate with our 0.60 $M_\odot$ models, *if* we use their assumption that the 215.2 s mode is the $k = 1$ mode. However, if the mode pattern of Clemens (1994) is significant, then the 215 s mode must be $k = 2$, and the hydrogen layer mass is closer to $1.5 \times 10^{-4} M_*$. The best way to settle this issue is to detect the predicted $l = 1$, $k = 1$ mode between 145–150 s, although we caution that a nondetection does not necessarily imply the 215 s mode must be $k = 1$. Another way is to determine the l identity of the modes near 120 and 200 s in G226–29, GD 165, and L19–2 in a manner similar to Robinson et al. (1995). If all of these stars have $l = 1$ modes at both periods, then we would have strong (albeit circumstantial) evidence that the 215 s mode in G117-B15A is the $k = 2$ mode.

TABLE 15

SEISMOLOGICAL MODEL MATCHES FOR G117-B15A: PURE CARBON CORES

OBJECT	$M_{\rm H}$ ($\times 10^{-4} M_*$)	$M_{\rm He}$ ($\times 10^{-2} M_*$)	$T_{\rm eff}$ (K)	MODE IDENTITY (1, 2)	(1, 3)	(1, 4)
G117-B15A.....	...	...	12,350	215.2	271.0	304.4
0.55 $M_\odot$	2.5	2.5	12,300	214.1	271.5	299.0
0.55 $M_\odot$	2.0	2.0	12,500	213.8	267.5	334.4
0.55 $M_\odot$	1.5	1.5	11,900	215.2	276.5	341.6

TABLE 16

SEISMOLOGICAL MODEL MATCHES FOR G117-B15A: C/O CORES

OBJECT	$M_{\rm H}/M_*$ ($\times 10^{-4} M_*$)	C/O MASS FRACTION	TRANSITION POINT (M_*)	$T_{\rm eff}$ (K)	MODE IDENTITY (1, 2)	(1, 3)	(1, 4)
G117-B15A.....	...	...	...	12,350	215.2	271.0	304.4
0.55 $M_\odot$	1.5	20:80	0.50	12,470	212.3	263.5	277.6
0.55 $M_\odot$	1.5	20:80	0.60	12,160	215.1	270.0	284.3
0.55 $M_\odot$	1.5	20:80	0.75	12,220	214.9	272.1	300.1
0.55 $M_\odot$	1.5	20:80	0.80	12,530	212.3	270.6	304.3
0.55 $M_\odot$	1.5	20:80	0.83	12,500	213.0	271.1	311.4
0.55 $M_\odot$	1.5	50:50	0.80	12,650	214.0	271.6	316.6
0.60 $M_\odot$	1.5	20:80	0.75	12,160	213.6	273.8	303.9[a]
0.55 $M_\odot$	1.5	20:80	0.75	12,970	215.4	280.8	300.6[a]
0.60 $M_\odot$	1.5	20:80	0.75	12,940	214.8	266.5[b]	306.8[a]

[a] Mode = (2, 8).
[b] Mode = (1, 4).

7. SUMMARY AND CONCLUSIONS

Our results for G117-B15A show that we should be able to perform asteroseismology on pulsating DA white dwarf stars and derive useful constraints on their internal structure. Constraining the mass of the hydrogen layer will be particularly valuable, given the controversy surrounding its thickness and the inability of nonadiabatic calculations (Cox et al. 1987; Bradley & Winget 1994a; Fontaine et al. 1994) and stellar evolution calculations (Iben 1989; D'Antona & Mazzitelli 1991) to constrain it. For seismological structural determinations, we emphasize comparisons between observed and calculated pulsation periods, because they are the quantities we measure most accurately from observations and calculate the most reliably with our models.

We provide tables containing pulsation periods for numerous $l = 1$ modes and some $l = 2$ modes for comparison to the observed periods of other DAV stars as reliable pulsation periods become available. In our grid, we assume hydrogen layer masses between $1.5 \times 10^{-4} M_*$ and $1.0 \times 10^{-6} M_*$. The tables will allow observers to examine a modest range of hydrogen layer masses around that suggested by Clemens (1994) and also test the theoretical prediction (Paczyński 1971; D'Antona & Mazzitelli 1979) that more massive white dwarfs should have smaller hydrogen layer masses.

If the hydrogen layer masses are of order $10^{-4} M_*$ in these stars, then we must consider the possible effects of quiescent hydrogen burning near the base of the H/He transition zone (Iben & MacDonald 1985, 1986) in future models. Hydrogen layer masses of $\sim 10^{-4} M_*$ in the DAV white dwarfs also suggest that the theory of how a star evolves from the asymptotic giant branch (AGB) to become a white dwarf (Iben & Tutukov 1984; Iben & MacDonald 1985, 1986; D'Antona & Mazzitelli 1991) is at least qualitatively correct. It would also imply that a minority of hot ($T_{\rm eff} \gtrsim 25{,}000$ K) DA white dwarfs have thin hydrogen layers ($M_{\rm H} \lesssim 10^{-10} M_*$) as required by spectral evolution theory (Fontaine & Wesemael 1987, 1991) to explain the "DB gap." The DB gap lies between 45,000 and 30,000 K, and there are no known DB white dwarfs lying within it—all white dwarfs in the DB gap have hydrogen photospheres.

While the work of Clemens (1994) offers an attractive solution to the hotter DAV stars where a few low-overtone modes are seen, it raises some questions when we try to perform seismology on cooler DAV stars where we see long-period modes. The biggest problem is trying to explain why we only see a few—of the many possible—long-period modes, especially since models with massive hydrogen layers predict more trapped modes than we observe. Higher overtone modes in our models show mode-trapping effects, but there is less kinetic energy contrast because most of the eigenfunction amplitude lies above the three mode-trapping interfaces. This relatively small kinetic energy contrast between long-period trapped and untrapped modes is the weak link in demonstrating that the cooler ZZ Ceti stars with a few long-period modes should have hydrogen layers with masses near $10^{-4} M_*$ as Clemens (1994) suggests. Proving this point is beyond the scope of this paper, but we note it as a problem that must eventually be addressed by white dwarf seismology.

Asteroseismology is fast proving itself to be a keen tool for probing the interior structures of the pulsating white dwarf stars. The Whole Earth Telescope collaboration was successful in determining many structural parameters of the DOV stars PG 1159−035 (Winget et al. 1991, Kawaler & Bradley 1994) and PG 2131+066 (Kawaler et al. 1995), and the DBV white dwarf GD 358 (Winget et al. 1994; Bradley & Winget 1994b). The models and tools described here will allow us to constrain the internal structure of the DA white dwarfs and, ultimately, their progenitors, an important step toward clarifying the differences in the origins of the DA and DB white dwarfs, along with refining the age of the local Galactic disk and constraining the physics of matter under extreme astrophysical conditions.

We are grateful to J. C. Clemens, C. J. Hansen, S. D. Kawaler, R. E. Nather, D. E. Winget, and M. A. Wood for their encouragement and many discussions. We also thank J. C. Clemens, J. A. Guzik, J. L. Provencal, D. E. Winget, and M. A. Wood for comments on earlier drafts of the manuscript. This research was supported by the National Science Foundation under grant 90-14655 through the University of Texas and McDonald Observatory and a Los Alamos National Laboratory Director's Postdoctoral Fellowship.

REFERENCES

Arcouragi, J.-P., & Fontaine, G. 1980, ApJ, 242, 1208
Bergeron, P., et al. 1993, AJ, 106, 1987
Bergeron, P., Saffer, R. A., & Liebert, J. 1992, ApJ, 394, 228
Bergeron, P., Wesemael, F., & Fontaine, G. 1992, ApJ, 387, 288
Bergeron, P., Wesemael, F., Lamontagne, R., Fontaine, G., Saffer, R. A., & Allard, N. F. 1995, ApJ, 449, 258
Bohm, K.-H., & Cassinelli, J. 1971, A&A, 12, 21
Bradley, P. A. 1993, Ph.D. thesis, Univ. Texas
Bradley, P. A., & Winget, D. E. 1991, ApJS, 75, 463
———. 1994a, ApJ, 421, 236
———. 1994b, ApJ, 430, 850
Bradley, P. A., Winget, D. E., & Wood, M. A. 1992, ApJ, 391, L33
———. 1993, ApJ, 406, 661
Bragaglia, A., Renzini, A., & Bergeron, P. 1993, in White Dwarfs: Advances in Observations and Theory, ed. M. A. Barstow (Dordrecht: Kluwer), 325
Brassard, P., Fontaine, G., Wesemael, F., & Hansen, C. J. 1992a, ApJS, 80, 369
Brassard, P., Fontaine, G., Wesemael, F. & Talon, A. 1993, in White Dwarfs: Advances in Observations and Theory, ed. M. A. Barstow (Dordrecht: Kluwer), 485
Brassard, P., Fontaine, G., Wesemael, F. & Tassoul, M. 1992b, ApJS, 81, 747
Brickhill, A. J. 1983, MNRAS, 204, 537
———. 1991, MNRAS, 251, 673
Clemens, J. C. 1994, Ph.D. thesis, Univ. Texas
Cox, A. N., Starrfield, S. G., Kidman, R. B., & Pesnell, W. D. 1987, ApJ, 317, 303
D'Antona, F., & Mazzitelli, I. 1979, A&A, 74, 161
———. 1991, in IAU Symp. 145, Evolution of Stars: the Photospheric Abundance Connection, ed. G. Michaud & A. Tutukov (Dordrecht: Kluwer), 399
Dziembowski, W. 1977, Acta Astron., 27, 203
Fontaine, G., & Brassard, P. 1994, in IAU Colloq. 147, The Equation of State in Astrophysics, ed. G. Chabrier & E. Schatzman (Cambridge: Cambridge Univ. Press), 347
Fontaine, G., Brassard, P., Bergeron, P., & Wesemael, F. 1992, ApJ, 399, L91
Fontaine, G., Brassard, P., & Wesemael, F. 1994, ApJ, 428, L61
Fontaine, G., & Wesemael, F. 1987, in IAU Colloq. 95, The Second Conference on Faint Blue Stars, ed. A. G. D. Philip, D. S. Hayes, & J. Liebert (Schenectady: Davis), 319

Fontaine, G., & Wesemael, F. 1991, in IAU Symp. 145, The Photospheric Abundance Connection, ed. G. Michaud & A. Tutukov (Dordrecht: Reidel), 421
Iben, I., Jr. 1989, in IAU Colloq. 106, Evolution of Peculiar Red Giant Stars, ed. H. R. Johnson & B. Zuckerman (Cambridge: Cambridge Univ. Press), 205
———. 1991, in IAU Symp. 145, The Photospheric Abundance Connection, ed. G. Michaud & A. Tutukov (Dordrecht: Reidel), 257
Iben, I., Jr., & MacDonald, J. 1985, ApJ, 296, 540
———. 1986, ApJ, 301, 164
Iben, I., Jr., & Tutukov, A. V. 1984, ApJ, 282, 615
Kawaler, S. D., & Bradley, P. A. 1994, ApJ, 427, 415
Kawaler, S. D., Hansen, C. J., & Winget, D. E. 1985, ApJ, 295, 547
Kawaler, S. D., et al. 1995, ApJ, 450, 350
Kepler, S. O. 1995, Baltic Astron., 4, 157
Kepler, S. O., et al. 1995, Baltic Astron., 4, 221
Kepler, S. O., & Nelan, E. P. 1993, AJ, 105, 608
Kepler, S. O., Robinson, E. L., Nather, R. E., & McGraw, J. T. 1982, ApJ, 254, 676
Koester, D., & Allard, N. 1993, in White Dwarfs: Advances in Observations and Theory, ed. M. A. Barstow (Dordrecht: Kluwer), 237
Koester, D., Allard, N. F., & Vauclair, G. 1994, A&A, 291, L9
Koester, D., & Schönberner, D. 1986, A&A, 154, 125
Lamb, D. Q., & Van Horn, H. M. 1975, ApJ, 200, 306
Paczyński, B. 1971, Acta Astron., 20, 47
Pfeiffer, B., et al. 1995, A&A, in press
Robinson, E. L., et al. 1995, ApJ, 438, 908
Robinson, E. L., Stover, R. J., Nather, R. E., & McGraw, J. T. 1978, ApJ, 220, 614
Stover, R. J., Hesser, J. E., Lasker, B. M., Nather, R. E., & Robinson, E. L. 1980, ApJ, 240, 865
Tassoul, M., Fontaine, G., & Winget, D. E. 1990, ApJS, 72, 335
van Altena, W. F., Lee, J. T., & Hoffleit, E. D. 1994, The General Catalogue of Trigonometric Parallaxes (New Haven: Yale Univ. Obs.)
Weseınael, F., Bergeron, P., Fontaine, G., & Lamontagne, R. 1991, in Proc. 7th European Workshop on White Dwarfs, ed. G. Vauclair & E. M. Sion (Dordrecht: Kluwer), 159
Winget, D. E., Hansen, C. J., Liebert, J., Van Horn, H. M., Fontaine, G., Nather, R. E., Kepler, S. O., & Lamb, D. Q. 1987, ApJ, 315, L77
Winget, D. E., et al. 1991, ApJ, 378, 326
———. 1994, ApJ, 430, 839
Wood, M. A. 1992, ApJ, 386, 539
Wood, M. A. 1995, in White Dwarfs, ed. D. Koester & K. Werner (Berlin: Springer), 41